Climate Change Projections for the Central Peruvian Coast (2006–2100) Using CMIP5 Models: Agricultural Impacts and Implications for the Growth of *Chenopodium quinoa* Willd in Arid Zones

Yvan Garcia-Lopez[1], Lía Ramos-Fernández[2], Luz Gomez-Pando[3]

ygarcia@lamolina.edu.pe

[1]PhD Program, Agraria La Molina National University, 15024 Lima, Peru

[2]Department of Water Resources, Agraria La Molina National University, 15024 Lima, Peru Environmental Engineering

[3]Cereal Research Program, Agraria La Molina National University, 15024 Lima, Peru

Abstract

We evaluated climatic data for the central coastal region of Peru (Lima) as simulated by the climate models used in the Coupled Model Intercomparison Project Phase 5 (CMIP5). The models were: MIROC-ESM, CSIRO Mk 3.6, CNRM-CM5, GFDL-CM3, IPSL-CM5A-MR, and MPI-ESM-LR, with respective spatial resolutions of 2.81° × 1.77°, 1.875° × 1.86°, 1.4° × 1.40°, 2.5° × 2.0°, 2.5° × 1.27°, and 1.875° × 1.875°. The models were built using observed meteorological data from this region for the 1975–2005 period and were employed under the IPCC's RCP2.6 and RCP8.5 scenarios.

The RCP2.6 and RCP8.5 scenarios were selected because they represent low and severe CO_2 concentration pathways, respectively. This approach allows for an assessment of the full range of potential climate impacts, from a future with ambitious mitigation (RCP2.6) to one with no mitigation intervention (RCP8.5). Thus, it provides a solid foundation for adaptation and mitigation decision-making, highlighting the urgency of climate action in the face of projected risks.

Using the Coupled Model Intercomparison Project Phase 5 (CMIP5) models, this study assesses their ability to predict mild and extreme climate events, as well as the critical implications for the agricultural sector. The analysis is particularly relevant for key crops in the area, such as asparagus (*Asparagus officinalis*), avocado (*Persea americana*), citrus fruits, grapevine (*Vitis vinifera*), maize (*Zea mays*), and the emerging and vulnerable quinoa (*Chenopodium quinoa* Willd.). Quinoa was specifically planted in an agricultural plot in La Molina, on the central coast of Lima, Peru, to evaluate its phenology, which could be affected by severe climate patterns until the end of the 21st century.

The results of this study reveal high variability among the models in the climate projections for the central region of Lima, with notable discrepancies in temperature and precipitation trends. The projections indicate significant warming, ranging from +1.2°C under the RCP2.6 scenario to +4.4°C under the RCP8.5 scenario, expected in the evaluated arid zone by the end of the century.

KEYWORDS: Climate models, CMIP5, RCP scenarios, climate projection, agricultural climatology, quinoa (*Chenopodium quinoa* Willd.), Peru.

1. Introduction

Global climate change

The planet's climate has historically maintained a balance due to its resilience. However, we are currently experiencing climate changes driven by increased concentrations of carbon dioxide (CO_2) and other greenhouse gases, generated by anthropogenic activities and fossil fuel consumption stimulated by economic and demographic growth. Consequently, among the temperatures recorded over the last 171 years on the Earth's surface, those from the period 1995-2006 were the warmest. Between 1906 and 2005, the planet's temperature showed a climatic variability increase of 0.74°C [1].

In 2018, the Intergovernmental Panel on Climate Change (IPCC) published a report on the impacts of global warming of 1.5°C under the best-case scenario and up to 2.0°C under the worst-case scenario for the next fifty years. IPCC reports present regional studies from climate models worldwide and outlines the most dramatic pathways for CO_2 and other greenhouse gas concentrations.

Climate changes, when they occur as extreme events, pose significant threats to ecosystems, economies, and societies, particularly those reliant on water resources for agriculture, livestock, and energy production [2-3].

Anthropogenic climate change, manifested through alterations in temperature and precipitation, is likely to pose a severe risk to human society, the economy, and ecosystems. It could lead to agricultural losses, water scarcity, widespread negative health impacts, and increased heat-induced mortality [4-5-6-7-8-9]. The effects of climate change are expected to be more severe in developing countries, as they depend on primary production as a major source of income [6].

Climate Systems

According to the National Centre for Atmospheric Research (NCAR), the climate system comprises the oceans, land, and atmosphere, as it integrates physicochemical processes within the atmosphere and interacts with the oceans, continents, ice, and

snow. It also includes fluxes from radiation, convection, and other processes. This system is represented using coupled models (Fig 1).

Climate models are classified into the following types: Global Circulation Models (GCMs), which encompass the entire planet, and Regional Climate Models (RCMs), which are confined to a specific climatic region. The information provided by GCMs has a resolution of approximately 100 to 200 km grid cells. This data is used to support decision-making at an international scale (for instance, in periodic IPCC meetings and reports) but is not considered suitable for decision-making for a specific country, let alone for a city [10]. These local climate scenarios, as they are called, carry considerable uncertainty.

Accurately simulating atmospheric phenomena plays a crucial role in understanding and predicting climate, especially in vulnerable regions such as the central coast of Peru. Climate specialists have managed to develop climate simulation models at smaller, local grid scales. This area, characterized by a strong ocean-atmosphere interaction, hosts highly productive marine ecosystems and communities that depend on stable climatic conditions [11].

In this context, the Coupled Model Intercomparison Project Phase 5 (CMIP5) has become an essential tool for assessing the predictive capability of global climate models [12-13]. It has been demonstrated that both the inherent complexity of these models and the degree of agreement among their simulations are key elements for estimating the reliability of their projections [14]. Climate scenarios have a significant margin of uncertainty; however, they are robust enough to be used in planning and policy formulation for human activities that need to be projected more than a decade into the future, such as forest management, water resource planning, urban development, agriculture, and tourism, among others [15].

Despite the progress achieved, significant knowledge gaps persist, particularly concerning the ability of models to predict extreme events and seasonal variations with high accuracy in specific regions. The need to enhance the understanding of climate projections for this area is critical, given its relevance for marine biodiversity and the local economy [16-17]. The coupled model intercomparison approach represents a robust strategy to address these limitations, as it enables a more rigorous assessment of model-associated uncertainty and facilitates the identification of both common patterns and significant divergences among simulations [18].

This study aimed to assess the complexity and level of agreement among CMIP5 atmospheric simulations applied to the central Peruvian coast using a coupled model intercomparison approach. To this end, an Intermodel Consensus Analysis was applied to quantify the degree of concordance among the ensemble projections. An index was calculated to identify areas where the models show coherence in the sign of climate trends and anomalies, and regions with significant discrepancies—such as differences in projected warming or cooling—were mapped. Furthermore, the Intermodel Coefficient of Variation was used to locate areas of higher uncertainty, such as winter cloud cover over Lima or summer temperature peaks [19-20].

The obtained results provided a more detailed perspective on the ability of CMIP5 models to represent the climate of the Peruvian coastal region, while also offering valuable information to improve future projections. The identification of shared patterns and areas of divergence advanced the understanding of the current limitations of the models and helped to propose new lines of research. This type of analysis is essential for designing effective adaptation strategies and mitigating the effects of climate change on coastal communities and marine ecosystems [21-22].

In the development of climate projections using Global Circulation Models (GCMs), the Coupled Model Intercomparison Project Phase 5 (CMIP5) has been made available. These Earth System Models (ESMs) incorporate the interactions of the atmosphere, land, and vegetation, in addition to accounting for the carbon cycle and atmospheric chemistry [12], unlike previous Phase 3 models. This new generation of models is driven by historical air composition forcing—recently defined as "historical forcing"—for current climate conditions, and by Representative Concentration Pathways (RCPs) for future scenarios [23].

In summary, the joint assessment of structural complexity and inter-model coherence in CMIP5 simulations constitutes a decisive step towards strengthening regional climate modeling capabilities [24]. Therefore, we will study two RCPs—RCP2.6 and RCP8.5 (representing a range of radiative forcing from lowest to highest by the year 2100)—using the following coupled models from the intercomparison project: MIROC-ESM, CSIRO-Mk3-6-0, CNRM-CM5, GFDL-CM3, IPSL-CM5A-MR, and MPI-ESM-LR. This work reaffirms the value of coupled intercomparison models [25] as key tools for reducing uncertainty and establishes a solid foundation for future research aimed at enhancing the climate resilience of the Peruvian coast.

2. Data and Study Area

Climate Model Data

This study presents an analysis of climate variables—specifically maximum and minimum temperatures and precipitation—for the period 2006-2100 in La Molina. It evaluates the effect of climatic conditions on the quinoa crop (*Chenopodium quinoa* Willd.) based on the calibration of historical data from the MIROC-ESM, CSIRO-Mk3-6-0, CNRM-CM5, GFDL-CM3, IPSL-CM5A-MR, and MPI-ESM-LR models, combined

with available observed historical data from the SENAMHI La Molina station for the period 1975-2005.

Table 1 *CMIP5 models used*

Model	Modeling Center (Origin)	Spatial resolution (Longitude × Latitude, degrees)	Ensemble
MIROC-ESM	Japón (AORI, NIES, JAMSTEC)	2.81° × 1.77°	r1i1p1
CSIRO Mk 3.6	Australia (CSIRO)	1.875° × 1.86°	r1i1p1
CNRM-CM5	Francia (CNRM, Météo-France)	1.41° × 1.40°	r1i1p1
GFDL-CM3	EE.UU. (NOAA/GFDL)	2.5° × 2.0°	r1i1p1
IPSL-CM5A-MR	Francia (IPSL)	2.5° × 1.27°	r1i1p1
MPI-ESM-LR	Alemania (Max Planck Institute)	1.875° × 1.875°	r1i1p1

Note. Compiled using information from the IPCC [33]

Table 1 shows the models used, along with their respective spatial resolutions and ensemble arguments. The study variables and their projections were processed using the downscaling method with the MeteoLab software; they were also evaluated using the paired Student's t-test and the Mann-Kendall test.

Study Area

Peru has a total area of 1,285,215 km² and comprises three distinct geographical regions: the coast, which accounts for 11% of the territory, the highlands (sierra) with 29%, and

the rainforest (selva) covering 60%. Politically, it is divided into 24 administrative regions (Fig 2).

The agroclimatic trial was conducted at the experimental agricultural plot of the Research and Social Outreach Program for Cereals and Native Grains, Faculty of Agronomy, National Agrarian University La Molina (UNALM). The site is located on the left margin of the Rímac River, in the Ate Bajo valley, La Molina district, Lima province, Lima region (Fig 3). Its geographical coordinates are Latitude: 12°05'06" S, Longitude: 76°57'06" W, at an altitude of 251 meters above sea level (m a.s.l.), corresponding to the Subtropical Desert formation, typical of the central Peruvian coast.

Indicates the location of the experimental plot, which is situated opposite the Botanical Garden. It should be noted that the average summer temperatures in La Molina range from 17°C to 31°C, while average winter temperatures fall within a range of 7°C to 23°C [26].

3. Methods

Delta method – linear scaling (LS)

In this study, the methods of correction as DELTA methods-linear scaling were used for precipitation and temperatures. This bias correction method was performed on a daily scale from 1975 to 2005.

The linear scaling approach operates under the assumption that forecast values and observations will agree in their monthly mean once a scale or shift factor has been applied [27]. LS is the simplest possible post-processing method as it only corrects for biases in the mean. The factor is commonly computed differently for precipitation, E_{T0} and temperature due to the different nature of the variables, as precipitation and E_{T0} cannot be negative.

For precipitation and E_{TO},

$$f^*_{k,i} = \frac{\sum_{j=1}^{N-1} yi}{\sum_{j=1}^{N-1} fi} f_{k,i} \qquad \text{for i} \neq \text{j}, \qquad (1)$$

For temperature

$$f^*_{k,i} = f_{k,i} - \frac{1}{N}\left[\sum_{J=1}^{N-1} f_j - \sum_{j=1}^{N-1} yj\right] \qquad \text{for i} \neq \text{j}, \qquad (2)$$

where $f_{k,i}$ denotes ensemble member k for $k = 1, \ldots, M$ of forecast–observation pair i = 1, . . . , N; N is the number of forecasts–observation pairs; f_j denotes the ensemble mean; and y_j denotes the verifying observation. Now, both the means of f_j and y_j are computed with the sample that withdraws forecast and observation pair i. Finally, $f^*_{k,i}$ represents the corrected ensemble member. Note that for precipitation, before applying the correction factor, we set all values of daily precipitation below a specific threshold to zero to remove the "drizzle effect" [28]. The threshold was chosen so that the number of dry days on a given forecast month matches the number of observed dry days.

Linear scaling (LS) of precipitation and temperature

The linear-scaling approach [29-30] operates with monthly correction values based on the differences between observed and present-day simulated values. By definition, corrected RCM simulations will perfectly agree in their monthly mean values with the observations. Precipitation is corrected with a factor based on the ratio of long-term monthly mean observed and control run data:

The Delta Change approach is based on the transfer of the average monthly change signal between the GCM control and the GCM scenario period at an observed time series:

$$T_{d,m}^{scen} = T_{d,m}^{obs} + (T_m^{GCMscen} - T_m^{GCMcon}) \quad (3)$$

$$P_{d,m}^{scen} = P_{d,m}^{obs} + (P_m^{GCMscen} / P_m^{GCMcon}) \quad (4)$$

where $T_{d,m}^{obs}$ y $P_{d,m}^{obs}$ daily temperature and precipitation are observed, T_m^{GCMcon} y P_m^{GCMcon} are average monthly temperature of GCM and precipitation of the control period, and $T_m^{GCMscen}$ y P_m^{GCMcon} are average monthly temperature of MCG and precipitation of the scenario period

Temperature is corrected with help of an additive term based on the difference of long-term monthly mean observed and control run data: The applied correction factors and addends are assumed to remain unvaried even for future conditions [31].

It should be emphasized that the climate change signals between the GCM baseline and the scenario period were derived from monthly mean values. This specific approach was chosen to avoid considerable variability in the daily change signals that would have resulted from using daily change factors.

Global climate models (CMIP5)

Projections for future climate change (RCP2.6 and RCP8.5)

This study will use two emission scenarios, or Representative Concentration Pathways (RCPs)—RCP2.6 (a mild scenario) and RCP8.5 (a severe scenario)—to assess greenhouse gas (GHG) emissions. The evaluation will be conducted using six coupled models from the Coupled Model Intercomparison Project Phase 5 (CMIP5): MIROC-ESM, CSIRO-Mk3-6-0, CNRM-CM5, GFDL-CM3, IPSL-CM5A-MR, and MPI-ESM-LR. These models will inform the agroclimatic trials for the quinoa crop (*Chenopodium quinoa* Willd.) conducted at the La Molina agricultural station.

An RCP is a representative pathway of CO_2 levels, each characteristic of a specific radiative forcing (RF). This forcing is caused by radiative agents and GHGs, excluding the direct effects of albedo. The term "pathway" indicates that not only the long-term CO_2 levels are of interest, but also the trajectory taken over time to reach that outcome [23]. These scenarios operate under a stable climate state, which requires an energy balance between incoming and outgoing terrestrial fluxes. According to the global energy balance, there is an excess of approximately 1 W/m² [32], which sustains temperatures that make life on Earth possible. However, a larger excess would result in increased climate warming.

The Fifth Assessment Report [33] considers four scenarios or Representative Concentration Pathways, developed using integrated assessment models as the basis for climate predictions and their respective projections. The Representative Concentration Pathways (RCPs) considered are:

- **RCP2.6:** A low radiative forcing pathway, peaking at approximately +2.6 W/m² before 2100, with emissions declining after 2020 and a projected warming peak of ~+1.5–2°C.
- **RCP8.5:** A high radiative forcing pathway, reaching values >8.5 W/m² by 2100, which continue to rise over time due to high emissions from intensive fossil fuel use, leading to a projected warming of ~+4–5°C by 2100.

Data Selection and Preparation

The precipitation (mm) and minimum and maximum temperature (°C) data used in this study were obtained from the Von Humboldt meteorological station, located at 12°00'05" S latitude and 76°57'00" W longitude, at an altitude of 243.7 meters above sea level (m a.s.l.), according to information from the Peruvian National Meteorology and Hydrology Service [34]. Furthermore, coupled models from the Coupled Model

Intercomparison Project Phase 5 (CMIP5) were employed, specifically: MIROC-ESM, CSIRO-Mk3-6-0, CNRM-CM5, GFDL-CM3, IPSL-CM5A-MR, and MPI-ESM-LR. These models are part of the suite of climate simulations developed by the World Climate Research Programme [11]. The models were selected for their ability to adequately represent the climatic conditions of the central Peruvian coast, particularly the La Molina area, which is characterized by a hot, arid subtropical desert climate [35]. A 30-year historical period (1975–2005) was considered as the climatic baseline, along with the period 2006–2100 for future projections. Additionally, it was verified that all selected models had an appropriate spatial resolution to capture local climatic particularities.

4. Discussion

Analysis of Climate Projections - Precipitation 1975-2005 vs 2006-2100

The behavior of the accumulated annual historical values (reference baseline) for the period 1975-2005, compared to that observed under the RCP2.6 (low emissions) and RCP8.5 (high emissions) scenarios for the six models in the assessed periods—2006-2035 (near future), 2036-2065 (mid-century), and 2066-2100 (far future)—is shown in Tables 1 and 3, respectively..

Table 2: Historical cumulative annual precipitation data for the period 1975-2005 and projected data from global climate models (RCP2.6) for the period 2006-2100.

	RCP2.6						
Periods	Pr Histórica	CNRM-CM5	CSIRO-Mk 3.6	GFDL-CM3	IPSL-CM5A-MR	MIROC-ESM	MPI-ESM-LR
1975-2005	422.98	-	-	-	-	-	-

2006-2035	-	377.03	357.96	349.89	2340.13	374.14	372.54
2036-2065	-	393.33	350.40	348.40	1875.10	396.78	384.42
2066 -2100	-	458.68	402.85	416.20	2733.00	440.00	457.46

In Table 2, it can be observed that the IPSL-CM5A-MR model shows extremely high values (~5-6 times higher than other models), suggesting a known overestimation by this model in coastal regions. In contrast, there is a degree of consistency among the other models, as most project a slight decrease in the near future (2006-2035) and an increase towards the end of the century (2066-2100), yet always remaining close to the historical value (422.98 mm). Under the RCP2.6 scenario, precipitation remains relatively stable, with potential moderate increases by 2100.

The graphic (Fig 4) presents the results for the RCP8.5 scenario, illustrating the behavior of the historical cumulative precipitation (1975-2005) versus the projections from the global climate models for the period 2006-2100.

Table 3 of the statistical tests for the historical data (1975-2005) shows that a high t-statistic (21.2) and a p-value ≈ 0 confirm that the mean is significantly different from zero. The Signal-to-Noise Ratio (SNR) is 0.20, indicating a weak signal relative to the noise, which is typical in arid climates like Lima's. Furthermore, a Hurst exponent (H) ≈ 0 denotes a highly anti-persistent series, characterized by abrupt changes between consecutive years.

Table 3. Paired Student's t-test for the cumulative historical annual precipitation values for the period 1975-2005 and the observed values from the RCP2.6 global climate models for the period 2006-2100.

Model	Pearson's R	t-statistic	P(T<=t) a queue	Coefficient of Variation	Signal-to-Noise	Hurst exponent

1975 -2005	0.1044	21.2147	0.000e+00	5.0141	0.1994	0.0017
CNRM-CM5	0.4990	36.5654	2.944e-287	5.0942	0.1963	0.0220
CSIRO Mk 3.6	0.4060	42.3332	0.000e+00	4.4001	0.2273	0.0440
GFDL-CM3	0.6360	36.3346	9.793e-284	5.1266	0.1951	0.0480
IPSL-CM5A-MR	0.6470	243.4333	0.000e+00	0.7652	1.3069	0.0470
MIROC-ESM	0.0560	36.6064	6.930e-288	5.0885	0.1965	0.0080
MPI-ESM-LR	0.2610	36.6668	9.805e-289	5.0808	0.1968	0.0090

The evaluated climate model IPSL-CM5A-MR (an outlier) shows a Pearson's R correlation coefficient of 0.647, which is the highest correlation with the historical record among all models. Its enormous t-statistic of 243.4 confirms its anomalous precipitation values (~5-6 times higher). An SNR of 1.31 indicates a strong signal dominant over the noise, which is unusual for precipitation data. Furthermore, a Hurst exponent (H) of 0.047 suggests a strongly anti-persistent series with a pronounced mean-reverting behavior, similar to the historical series.

For the GFDL-CM3 and CNRM-CM5 models (considered consistent models), the analysis shows a Pearson's R correlation coefficient of approximately 0.5-0.6, indicating a moderate to high correlation with the historical record. The t-statistic, with values around 36-37, confirms that the means are significantly different from zero, though not to an extreme degree. The Signal-to-Noise Ratio (SNR) of approximately 0.19-0.20 reflects a weak signal, which is consistent with the historical data. Finally, a Hurst

exponent (H) of about 0.02-0.05 suggests a short-term memory process (anti-persistent), a characteristic similar to the historical series.

Finally, for the CSIRO-Mk3-6-0, MIROC-ESM, and MPI-ESM-LR models (considered conservative models), the Pearson's R correlation coefficient ranges from approximately 0.06 to 0.41, indicating a low to moderate correlation with the historical record. The t-statistic, with values between approximately 36 and 43, confirms a statistically significant difference from the historical mean. The Signal-to-Noise Ratio (SNR) of approximately 0.20-0.23 reflects a weak signal, consistent with the historical data. A Hurst exponent (H) ranging from 0.008 to 0.044 denotes a strongly anti-persistent, mean-reverting series.

Table 4. Historical cumulative annual precipitation data for the period 1975-2005 and projected data from global climate models (RCP8.5) for the period 2006-2100.

	RCP8.5						
Periods	Historical baseline	CNRM-CM5	CSIRO Mk 3.6	GFDL-CM3	IPSL-CM5A-MR	MIROC-ESM	MPI-ESM-LR
1975-2005	422.98	-	-	-	-	-	-
2006-2035	-	355.75	356.76	144.07	1314.22	384.42	385.48
2036-2065	-	373.56	365.30	276.57	2308.15	378.42	387.79
2066 - 2100	-	473.71	380.75	399.92	1591.71	441.23	431.04

Table 4 presents the projections for the RCP8.5 scenario (characterized by high radiative forcing and unmitigated emissions). The comparison begins with the historical baseline (422.98 mm), revealing that all models project significant changes in precipitation under RCP8.5. The IPSL-CM5A-MR model again shows extremely high

values (an outlier), consistent with its behavior under the RCP2.6 scenario.

Furthermore, the GFDL-CM3 model projects a drastic reduction in the near future (2006-2035: 144.06 mm, representing a -66% change versus the historical baseline).

The trends for the global climate models for the period 2006-2035 (Near Future) show moderate reductions for CNRM-CM5 (-16%), CSIRO-Mk3-6-0 (-16%), MIROC-ESM (-9%), and MPI-ESM-LR (-9%). In contrast, an extreme reduction is projected by GFDL-CM3 (-66%), while IPSL-CM5A-MR projects an extreme increase (+211%).

For the 2036-2065 period (Mid-Century), a partial recovery is observed. GFDL-CM3 shows an increase (276.57 mm) but remains below the historical baseline (-35%). IPSL-CM5A-MR reaches its peak value (2308.15 mm, +446%). The other models remain stable or show slight reductions.

Finally, for the 2066-2100 period (Long-Term Future), the greatest variability is seen in GFDL-CM3, which recovers to nearly historical levels (399.92 mm, -5%). IPSL-CM5A-MR decreases but remains very high (1591.71 mm, +276%). Moderate increases are projected for CNRM-CM5 (+12%), MIROC-ESM (+4%), and MPI-ESM-LR (+2%), while CSIRO-Mk3-6-0 remains stable (-10%).

The graphic (Fig 5) presents the results for the RCP8.5 scenario, illustrating the behavior of the historical cumulative precipitation (1975-2005) versus the projections from the global climate models for the period 2006-2100.

Table 5 of the global climate models under the RCP8.5 scenario aids in interpreting the statistical results. It demonstrates that all models, except for the GFDL-CM3, maintain a Hurst exponent (H) close to zero. This confirms that precipitation in Lima follows a mean-reverting pattern, where dry and wet years tend to alternate. In contrast, the GFDL-CM3 model shows an H value of 0.37, the highest among all models, suggesting a degree of persistence and a potential overestimation of prolonged drought conditions.

Tabla 5. Prueba T de Student pareada para los valores de precipitación anual histórica acumulada para el periodo del 1975-2005 y las proyectadas de los modelos climáticos globales RCP8.5 para el periodo 2006-2100.

Model	Pearson's R	Statistic-t	P(T<=t) a queue	Coefficient of Variation	Signal-to-Noise	Hurst exponent
1975 -2005	0.1044	21.2147	0.000e+00	5.0141	0.1994	0.0017
CNRM-CM5	0.5020	36.7681	2.287e-290	5.0661	0.1974	0.0200
CSIRO Mk 3.6	0.4140	42.1042	0.000e+00	4.4241	0.226	0.0410
GFDL-CM3	0.9960	46.5798	0.000e+00	3.999	0.2501	0.3700
IPSL-CM5A-MR	0.5020	215.0703	0.000e+00	0.8661	1.1546	0.0130
MIROC-ESM	0.0430	36.7473	4.772e-290	5.069	0.1973	0.0040
MPI-ESM-LR	0.2520	36.8021	6.849e-291	5.0614	0.1976	0.0130

Regarding the Signal-to-Noise Ratio (SNR), the IPSL-CM5A-MR model again stands out with a value of 1.15, indicating a strong signal dominant over the noise, which is consistent with its extreme projected rainfall values. The other models maintain an SNR of approximately 0.20, similar to the historical value (0.19), reflecting high interannual uncertainty.

The IPSL-CM5A-MR model has the lowest coefficient of variation (CV) at 0.87%, confirming low variability, which corresponds to its projection of constantly high rainfall. The GFDL-CM3 model projects greater stability (CV = 4.0% vs. a historical

value of 5.01%), a characteristic possibly resulting from a reduction in extreme precipitation events. All p-values are approximately zero ($p \approx 0$), indicating that the differences between the historical mean and the future projections are statistically significant. Concerning the correlation with the historical record (Pearson's R), the GFDL-CM3 model shows the highest value (0.996), suggesting its projections closely follow historical patterns despite the overall reduction in mean precipitation. In contrast, the MIROC-ESM model has the lowest correlation (0.043), indicating major deviations from the observed historical behavior.

Among all models evaluated under both the RCP2.6 and RCP8.5 scenarios, the IPSL-CM5A-MR model projects substantially greater precipitation increases than the others. This behavior is potentially associated with its high climate sensitivity and the representation of convective processes. Although these values could be interpreted as extreme outliers, they remain useful for assessing high-risk scenarios.

Time Series Analysis of Precipitation: Historical Baseline (1975–2005) and Future Projections (2006–2100)

The graphics (**Fig 6A, 6B,** and **6C**), corresponding to the CNRM, CSIRO, and GFDL models, show that annual precipitation in La Molina exhibits a clear divergence depending on the emission scenario. Under RCP2.6, which represents ambitious mitigation, the models project a generally stable trend or slight variations, suggesting a degree of hydrological cycle stabilization. In contrast, under the high-emissions RCP8.5 scenario, all three models concur in projecting a significant increase in accumulated precipitation, indicating an intensification of the rainfall regime for La Molina. This divergence underscores the profound influence of emission trajectories on the future climate, highlighting how mitigation actions are crucial to avert more extreme changes in precipitation patterns.

Table 6. Non-parametric test (Sen-Mann-Kendall slope test) for precipitation values obtained using the DELTA correction method in the CNRM, CSIRO, and GFDL models, for the period 2006-2100.

Model	S	Z	Sen´s Slope	Significance	Trend
CNRM RCP2.6	270929	0.126	0	insignificant	No significant trend at 95%
CNRM RCP8.5	1551834	0.720	0	insignificant	No significant trend at 95%
CSIRO RCP2.6	-2057071	-0.955	0	insignificant	No significant trend at 95%
CSIRO RCP8.5	-2560256	-1.188	0	insignificant	No significant trend at 95%
GFDL RCP2.6	-266291	-0.124	0	insignificant	No significant trend at 95%
GFDL RCP8.5	17062862	7.920	0	significant	Positive trend at 95%

The Mann-Kendall test results presented in Table 6 indicate that precipitation projections for quinoa cultivation in La Molina are predominantly stable, suggesting no drastic changes in irrigation water availability are expected under most scenarios. However, the significant positive trend projected by the GFDL model under RCP8.5 signals potential extreme rainfall events. This could increase the risk of flooding, waterlogging, and fungal diseases in the crop, ultimately affecting its yield and quality. This divergence underscores the need to implement flexible adaptation strategies—such as improved drainage systems and the selection of quinoa varieties resistant to both dry and humid conditions—to ensure crop sustainability in the face of climate uncertainty. The climate projections for precipitation shown (**Fig 7A, 7B** and **7C**) for the IPSL, MIROC, and MPI models reveal a clear divergence between emission scenarios. Under RCP2.6, the models project generally stable trends or moderate fluctuations, indicating a relative stability in La Molina's precipitation regime if mitigation measures are applied.

In contrast, the high-emissions RCP8.5 scenario shows a more extreme and variable response: the IPSL model suggests a pronounced increase, MIROC projects a markedly ascending trend, and MPI indicates a slight positive or stable trend. This inter-model discrepancy under RCP8.5 highlights the uncertainties in precipitation projections, yet it converges in indicating more drastic and potentially disruptive changes to the hydrological cycle in the absence of mitigation.

Table 7: Non-parametric test (Sen-Mann-Kendall slope test) for precipitation values obtained using the DELTA correction method in the IPSL, MIROC, and MPI models, for the period 2006-2100.

Model	S	Z	Sen´s Slope	Significance	Trend
IPSL RCP2.6	7123892	3.307	0	significant	Positive trend at 95%
IPSL RCP8.5	-8620281	-4.001	0	significant	Positive trend at 95%
MIROC RCP2.6	-450039	-0.209	0	insignificant	No significant trend at 95%
MIROC RCP8.5	1711984	0.795	0	insignificant	No significant trend at 95%
MPI RCP2.6	-831221	-0.386	0	insignificant	No significant trend at 95%
MPI RCP8.5	-179535	-0.083	0	insignificant	No significant trend at 95%

The Mann-Kendall test results for the IPSL, MIROC, and MPI models, presented in Table 7, reveal that only the IPSL model projects significant trends in precipitation, showing an increase under RCP2.6 and a critical decrease under RCP8.5. This pronounced decline under the high-emissions scenario (RCP8.5) would suggest increased water stress for quinoa cultivation in La Molina, potentially reducing water availability during key growth stages. In contrast, the MIROC and MPI models show no significant trends, indicating that, according to these models, the rainfall regime would remain stable without drastic changes.

This discrepancy underscores a high degree of uncertainty in the projections. However, the negative signal from IPSL—the most extreme model—serves as a warning: should

emissions follow the RCP8.5 trajectory, quinoa could face severe drought-related challenges, necessitating adaptation strategies such as supplemental irrigation or the selection of resistant varieties.

Analysis of Climate Projections - Minimum Temperature

1975-2005 vs 2006-2100

The behavior of the historical baseline minimum temperatures (1975-2005) compared to the projections under the RCP2.6 (low emissions) and RCP8.5 (high emissions) scenarios is presented in Tables 8 and 10, respectively. The data from six models are shown for the evaluated periods: 2006-2035 (near future), 2036-2065 (mid-century), and 2066-2100 (long-term future).

Table 8. Average historical minimum temperature for the period 1975-2005 and observed data from global climate models RCP2.6 for the period 2006-2100.

	RCP2.6						
Periods	Historical Baseline	CNRM-CM5	CSIRO-Mk 3.6	GFDL-CM3	IPSL-CM5A-MR	MIROC-ESM	MPI-ESM-LR
1975-2005	16.09	-	-	-	-	-	-
2006-2035	-	16.71	17.12	17.03	16.79	16.78	17.08
2036-2065	-	17.15	17.86	16.98	17.18	17.58	17.51
2066 -2100	-	17.15	18.14	17.10	17.10	17.79	17.24

In the table 8 the historical minimum temperature (16.09°C) in La Molina (central coast) is projected to increase by approximately +1.4°C by the period 2066-2100 (multi-model mean: 17.49°C). Projections indicate a consistent rise until 2065, after which temperatures stabilize or exhibit minimal growth; for instance, the CNRM-CM5 model shows no change between the 2036-2065 and 2066-2100 periods. While the models show a range of 17.10°C to 18.14°C, all indicate a clear warming trend. The CSIRO-

Mk3-6-0 model projects the greatest sensitivity, with an increase of +2.05°C relative to the historical baseline.

The graphic presents (Fig 8) the results for the RCP2.6 scenario, illustrating the behavior of the average historical minimum temperature (1975-2005) in comparison to the projections from the global climate models for the period 2006-2100.

The implications of this scenario include a reduction in nocturnal frost events and a potential decrease in extreme cold events. However, the potential impact on cold-sensitive crops cultivated in the central coast must be considered, with the notable exception of quinoa (*Chenopodium quinoa* Willd.). An improvement in nocturnal thermal comfort is also projected.

Table 9. Paired Student's t-test for historical average annual minimum temperature values for the period 1975-2005 and projected values from the RCP2.6 global climate models for the period 2006-2100.

Models	Pearson's R	Statistic-t	P(T<=t) a queue	Coefficient of Variation	Signal-to-Noise	Hurst exponent
Historical Baseline	0.9210	632.6308	0.000e+00	0.1682	5.9455	0.2330
CNRM-CM5	0.9270	1109.3002	0.000e+00	0.1679	5.9553	0.2540
CSIRO Mk 3.6	0.9220	1159.1228	0.000e+00	0.1607	6.2228	0.2680
GFDL-CM3	0.9510	872.1064	0.000e+00	0.2136	4.6819	0.3450
IPSL-CM5A-MR	0.9240	1137.2999	0.000e+00	0.1638	6.1056	0.2390
MIROC-ESM	0.9200	1193.2386	0.000e+00	0.1561	6.4059	0.2390
MPI-ESM-LR	0.9220	1160.6077	0.000e+00	0.1605	6.2307	0.2540

In table 9, 1975-2005 reference period serves as a benchmark for comparison with climate models under a low-emission scenario. The analysis indicates that most models project a decrease in variability (lower Coefficient of Variation) and an increase in the Signal-to-Noise Ratio (SNR) compared to the historical period. This suggests the potential for more stable and well-defined climatic projections. The Hurst exponent,

which quantifies long-term persistence, increases across all models, particularly in GFDL-CM3. This indicates a more pronounced trend and a greater influence of external forcings on the future climate system. The very high correlation (Pearson's R) and statistical significance ($p \approx 0$) in all cases confirm the robustness of the trends projected by the models.

Table 10. Average historical minimum temperature for the period 1975-2005 and projected temperatures from global climate models (RCP8.5) for the period 2006-2100

	RCP8.5						
Periods	Historical Baseline	CNRM-CM5	CSIRO-Mk 3.6	GFDL-CM3	IPSL-CM5A-MR	MIROC-ESM	MPI-ESM-LR
1975-2005	16.09	-	-	-	-	-	-
2006-2035	-	16.78	17.21	16.79	17.06	16.92	17.31
2036-2065	-	17.83	18.85	17.97	18.43	18.37	18.82
2066 - 2100	-	19.45	21.19	19.42	20.56	20.39	20.86

Table 10 reveals a dramatic increase in the average minimum temperature, rising from a historical value of 16.09°C to a multi-model mean of 20.32°C for the period 2066-2100, representing an increase of +4.14°C. This accelerated growth indicates a non-linear warming pattern. The temperature rise between the 2036-2065 and 2066-2100 periods is +1.77°C, suggesting a significant acceleration of climate change impacts in the latter half of the century.

Considerable inter-model variability is evident. The GFDL-CM3 model projects the most conservative warming (+3.33°C), while the CSIRO-Mk3-6-0 model projects the most extreme increase (+5.10°C). The most sensitive models—CSIRO-Mk3-6-0, IPSL-

CM5A-MR, and MPI-ESM-LR—all project minimum temperatures exceeding 20°C by the end of the 21st century.

The results for the RCP8.5 scenario (Fig 9), compare the average historical minimum temperature from 1975-2005 with the projections of global climate models for 2006-2100.

The critical implications of these projections include the virtual elimination of cool nights in cities like La Molina, which currently experiences a temperate coastal climate. Nights with minimum temperatures exceeding 20°C will become the norm, effectively removing the period of nocturnal thermal relief. This warming is projected to disrupt the biological cycles of native flora and fauna. Furthermore, for urban and peri-urban agriculture, there is a significant risk of crop loss for species that require cold periods for flowering and vernalization, such as certain fruits and vegetables cultivated in the central coast.

Table 11. Paired Student's t-test for historical average annual minimum temperature values for the period 1975-2005 and projected values from global climate models (RCP8.5) for the period 2006-2100.

Models	Pearson's R	Statistic-t	P(T<=t) a queue	Coefficient of Variation	Signal-to-Noise	Hurst exponent
Historical Baseline	0.9210	632.6308	0.000e+00	0.1682	5.9455	0.2330
CNRM-CM5	0.9390	1079.2975	0.000e+00	0.1726	5.7942	0.256
CSIRO Mk 3.6	0.9420	1084.8489	0.000e+00	0.1717	5.824	0.257
GFDL-CM3	0.9530	905.429	0.000e+00	0.2057	4.8608	0.342
IPSL-CM5A-MR	0.9430	1079.8644	0.000e+00	0.1725	5.7973	0.243
MIROC-ESM	0.9370	1133.8597	0.000e+00	0.1643	6.0871	0.229
MPI-ESM-LR	0.9390	1134.0341	0.000e+00	0.1643	6.0881	0.244

Under the high-emissions RCP8.5 scenario presented in Table 11, the contrast with the 1975-2005 historical baseline is more pronounced. The models generally show a

slightly higher Pearson correlation coefficient (r) compared to the results in Table 7, indicating a stronger, more linear relationship with radiative forcing. Although the variability, as measured by the Coefficient of Variation, is greater than under the low-emissions RCP2.6 scenario, the Signal-to-Noise ratio remains high. This implies that the warming signal is extremely strong and clear against the backdrop of natural variability. The Hurst Exponent remains elevated, confirming a strong persistence in the warming trend, with the GFDL-CM3 model again exhibiting the highest value, which suggests potentially more irreversible and long-term climate changes.

Time Series Analysis Minimum Temperature: Historical Baseline (1975–2005) and Future Projections (2006–2100)

The projections in (**Fig 10A, 10B,** and **10C**) from the CNRM, CSIRO, and GFDL models indicate a consistent increase in annual minimum temperature under both scenarios, with a more pronounced rise under RCP8.5. By 2100, RCP2.6 shows a stabilization of temperatures after mid-century, reflecting the effects of mitigation, whereas RCP8.5 exhibits an accelerated and relentless warming trajectory. This sustained warming, particularly in minimum temperatures, suggests warmer winters and a reduced frequency of frost events, which could disrupt crucial vernalization periods for some crops. However, it also entails risks such as the proliferation of pests and increased thermal stress on plants. The critical divergence between scenarios underscores the urgency of mitigation to avoid the most severe impacts on agriculture.

Table 12. Non-parametric test (Sen-Mann-Kendall slope test) for minimum temperature values obtained using the DELTA correction method in the CNRM, CSIRO, and GFDL models, for the period 2006-2100.

Model	S	Z	Sen´s Slope	Significance	Trend
CNRM RCP2.6	29558439	13.719	8.93714E-06	significant	Positive trend at 95%

CNRM RCP8.5	157736161	73.213	0.000111317	significant	Positive trend at 95%
CSIRO RCP2.6	65953870	30.612	2.63959E-05	significant	Positive trend at 95%
CSIRO RCP8.5	230286222	106.887	0.000183539	significant	Positive trend at 95%
GFDL RCP2.6	8053662	3.738	-5.36557E-06	significant	Positive trend at 95%
GFDL RCP8.5	110901878	51.475	0.000102636	significant	Positive trend at 95%

The global CSIRO and GFDL models presented in Table 12 indicate a consistent and statistically significant warming trend across all scenarios (RCP2.6 and RCP8.5) for the 2006-2100 period. This increase in minimum temperatures, which is particularly more accelerated under the high-emissions scenario (RCP8.5), suggests warmer winters and a reduction of frost events in La Molina. For quinoa cultivation, this could shorten the period of vernalization (the cooling required for flowering), alter its phenological cycle, and increase the risk of thermal stress during warm nights, potentially affecting grain yield and quality. However, it would also reduce the risk of frost damage, allowing for a more flexible planting window. Adaptation would require selecting heat-tolerant quinoa varieties and adjusting planting dates to optimize crop development in a warmer climate.

The graphics (**Fig 11A, 11B** and **11C**) for the IPSL, MIROC, and MPI models project an unequivocal and accelerated increase in the annual minimum temperature under both scenarios, with warming being dramatically more intense under RCP8.5. By the end of the century, RCP2.6 shows a stabilization of temperatures, whereas RCP8.5, across all models, presents a relentless upward trajectory that does not plateau. This sustained warming of night-time temperatures suggests the virtual disappearance of frost events in the region, which would profoundly alter the cold requirements (vernalization) of crops such as quinoa. While the risk of frost is reduced, this introduces greater nocturnal thermal stress and a potential increase in the evapotranspiration rate. The critical

divergence between scenarios emphasizes that mitigation is crucial to avoid severe impacts on crop physiology and traditional agricultural cycles.

Table 13. Non-parametric test (Sen-Mann-Kendall slope test) for minimum temperature values obtained using the DELTA correction in the IPSL, MIROC, and MPI models, for the period 2006-2100.

Model	S	Z	Sen´s Slope	Significance	Trend
IPSL RCP2.6	22107641	10.261	3.79848E-06	significant	Positive trend at 95%
IPSL RCP8.5	195621129	90.797	0.000150932	significant	Positive trend at 95%
MIROC RCP2.6	63746118	29.588	3.05972E-05	significant	Positive trend at 95%
MIROC RCP8.5	207198221	96.170	0.000158246	significant	Positive trend at 95%
MPI RCP2.6	6296781	2.923	-1.48923E-05	significant	Positive trend at 95%
MPI RCP8.5	206932153	96.047	0.000154378	significant	Positive trend at 95%

The Mann-Kendall test results in Table 13 confirm a significant and consistent warming trend in the minimum temperature for all models (IPSL, MIROC, MPI) and scenarios (RCP2.6 and RCP8.5) in La Molina. This increase, which is especially drastic under RCP8.5, implies warmer nights and the virtual elimination of frost events, thereby altering the crucial vernalization cycle for quinoa, a crop that requires cold for adequate flowering. While the risk of frost damage is reduced, persistent nocturnal heat can accelerate phenological development, reduce productivity, and increase water stress due to higher evapotranspiration. To adapt, it will be essential to select heat-tolerant quinoa varieties and adjust planting dates to avoid critical periods of thermal stress, ensuring the sustainability of the crop in a warmer climate.

Analysis of Climate Projections - Maximum temperature

1975-2005 vs 2006-2100

The behavior of the historical maximum temperature values (reference baseline, 1975-2005) compared to those observed under the RCP2.6 (low emissions) and RCP8.5 (high

emissions) scenarios for the six models—across the assessed periods of 2006-2035 (near future), 2036-2065 (mid-century), and 2066-2100 (far future)—is presented in Tables 14 and 16, respectively.

Table 14. Average historical maximum temperature for the period 1975-2005 and observed data from global climate models (RCP2.6) for the period 2006-2100.

	RCP2.6						
Periods	Historical Baseline	CNRM-CM5	CSIRO-Mk 3.6	GFDL-CM3	IPSL-CM5A-MR	MIROC-ESM	MPI-ESM-LR
1975-2005	23.29	-	-	-	-	-	-
2006-2035	-	23.80	24.10	24.40	24.50	24.10	22.80
2036-2065	-	24.10	25.10	24.60	24.70	25.20	23.20
2066 -2100	-	24.00	25.30	24.40	24.60	25.50	23.00

Table 14 shows that the historical maximum temperature (23.29°C) in La Molina increases by approximately +1.2°C by the period 2066-2100 (multi-model mean: 24.47°C). Projections indicate a steady rise until 2065, followed by a stabilization or even a slight decrease (for instance, GFDL-CM3 and MPI-ESM-LR project a reduction in the final period). The models show a range of 23.00°C to 25.50°C, yet all indicate a clear increase relative to the historical baseline. The MIROC-ESM model is the most sensitive, projecting an increase of +2.21°C above the historical value.

The results for the RCP2.6 scenario (Fig 12), compare the average historical maximum temperature from 1975-2005 with the projections of global climate models for 2006-2100.

The implications of this low-emissions scenario include moderate warming that would likely alter crop development slightly and necessitate adjustments in water management, but without extreme changes in maximum temperatures.

Table 15. Paired Student's t-test for historical average annual maximum temperature values for the period 1975-2005 and projected values from the RCP2.6 global climate models for the period 2006-2100.

Models	Pearson's R	Statistic-t	P(T<=t) a queue	Coefficient of Variation	Signal-to-Noise	Hurst exponent
Historical Baseline	0.9000	631.0209	0.000e+00	0.1686	5.9301	0.2110
CNRM-CM5	0.8939	1046.9823	0.000e+00	0.1779	5.6207	0.1360
CSIRO Mk 3.6	0.9210	1030.3005	0.000e+00	0.1808	5.5312	0.2600
GFDL-CM3	0.9160	1044.2679	0.000e+00	0.1784	5.6062	0.2660
IPSL-CM5A-MR	0.9080	1108.860	0.000e+00	0.1680	5.9529	0.2270
MIROC-ESM	0.9030	1153.0624	0.000e+00	0.1615	6.1902	0.2310
MPI-ESM-LR	0.9170	985.2139	0.000e+00	0.1891	5.2891	0.2470

Table 15, under this low-emissions scenario (RCP2.6), reveals a moderate behavior when compared to the 1975-2005 historical period. Most models show a Pearson correlation coefficient (r) that is slightly lower or similar to the historical baseline, suggesting that the relationship with radiative forcing, while still very strong, is less linear than under the high-emissions scenario shown in Table 13. A slight increase in variability (Coefficient of Variation) and a corresponding decrease in the Signal-to-Noise ratio are observed compared to the baseline period. This indicates that the warming signal, although clear, is more influenced by internal climate variability. The Hurst Exponent values, generally lower than those in the high-emissions scenario of Table 15 (particularly for the CNRM-CM5 model), point to reduced long-term persistence. This suggests that climate changes could be more manageable and potentially less irreversible if emissions are mitigated.

Table 16: Average historical maximum temperature for the period 1975-2005 and observed data from global climate models (RCP8.5) for the period 2006-2100.

	RCP2.6						
Periods	Tmax Baseline	CNRM-CM5	CSIRO-Mk 3.6	GFDL-CM3	IPSL-CM5A-MR	MIROC-ESM	MPI-ESM-LR
1975-2005	23.29	-	-	-	-	-	-
2006-2035	-	23.90	24.00	24.50	24.20	24.30	22.90
2036-2065	-	24.60	26.10	25.50	25.50	25.90	24.30
2066 -2100	-	25.50	27.90	26.80	27.70	28.00	26.30

In the table 16, the historical maximum temperature (23.29°C) in La Molina increases drastically by approximately +4.4°C by the 2066-2100 period (multi-model mean: 27.7°C). In contrast to the other scenario, the projections show an accelerated and consistent rise in each period, with no signs of stabilization. The models exhibit a wide range of 25.5°C to 28.0°C, yet all converge on a trajectory of severe warming. The MIROC-ESM model is again the most sensitive, projecting an increase of +4.71°C relative to the historical baseline.

The graphic presents the results for the RCP8.5 scenario (Fig 13), showing the behavior of the average historical maximum temperature (1975-2005) versus the projection from the global climate models for 2006-2100.

The implications of this high-emissions scenario are severe and include a high risk of crop thermal stress, increased evapotranspiration that would severely impact water resources, and more intense and frequent heatwaves.

Table 17. Results of the paired Student's t-test for average annual historical maximum temperature values (1975–2005) versus those projected by global climate models under the RCP8.5 scenario (2006–2100

Models	Pearson's R	Statistic-t	P(T<=t) a queue	Coefficient of Variation	Signal-to-Noise	Hurst exponent
1975 -2005	0.9000	631.0209	0.000e+00	0.1686	5.9301	0.2110
CNRM-CM5	0.835	1070.7394	0.000e+00	0.1740	5.7483	0.1290

CSIRO Mk 3.6	0.936	975.1151	0.000e+00	0.1910	5.2349	0.2710
GFDL-CM3	0.915	1100.0942	0.000e+00	0.1693	5.9059	0.2550
IPSL-CM5A-MR	0.922	1083.6282	0.000e+00	0.1719	5.8175	0.2320
MIROC-ESM	0.909	1169.0966	0.000e+00	0.1593	6.2763	0.2190
MPI-ESM-LR	0.920	1034.8161	0.000e+00	0.1800	5.5554	0.2470

Under the high-emissions RCP8.5 scenario presented in Table 17, the contrast with the 1975-2005 historical period is more pronounced. The models generally exhibit a slightly higher Pearson correlation coefficient (r) than that observed under the RCP2.6 scenario (Table 10), indicating a stronger and more linear relationship with radiative forcing. Although the variability, measured by the Coefficient of Variation, is greater than in the historical period, the Signal-to-Noise ratio remains very high. This signifies that the warming signal is extremely strong and clear against the background of natural variability. The Hurst Exponent remains elevated in most models, confirming a strong persistence in the warming trend. The CSIRO-Mk3-6-0 model shows the highest persistence value (0.271), suggesting potentially more irreversible and long-term climate changes where warming trends are strongly entrenched

Time Series Analysis Maximun Temperature: Historical Baseline (1975–2005) and Future Projections (2006–2100)

The graphics (**Fig 14A, 14B,** and **14C**) for the CNRM, CSIRO, and GFDL models project a consistent increase in the maximum temperature for the 2006-2100 period, with a clear divergence between scenarios. Under RCP2.6, warming moderates after mid-century, reflecting the effects of mitigation, whereas under RCP8.5 the increase is accelerated and sustained until 2100. This exacerbated warming implies more frequent and intense heatwaves, which would increase thermal stress on crops such as quinoa, elevating the evapotranspiration rate and water demand. The critical difference between

scenarios underscores the urgency of reducing emissions to avoid severe impacts on agriculture and water availability.

Table 18. Non-parametric test (Sen-Mann-Kendall slope test) for minimum temperature values obtained using the DELTA correction in the CNRM, CSIRO, and GFDL models, for the period 2006-2100.

Model	S	Z	Sen´s Slope	Significance	Trend
CNRM RCP2.6	15128407	7.022	6.2383E-06	significant	Positive trend at 95%
CNRM RCP8.5	72838942	33.808	8.02828E-05	significant	Positive trend at 95%
CSIRO RCP2.6	48864105	22.680	4.2249E-05	significant	Positive trend at 95%
CSIRO RCP8.5	141356718	65.610	0.00017748	significant	Positive trend at 95%
GFDL RCP2.6	8296607	3.851	4.14665E-06	significant	Positive trend at 95%
GFDL RCP8.5	101689102	47.199	0.00011058	significant	Positive trend at 95%

The Mann-Kendall test results in Table 18 confirm a significant and accelerated warming trend in the maximum temperature for all models (CNRM, CSIRO, GFDL) and scenarios (RCP2.6 and RCP8.5) in La Molina. This increase, which is particularly intense under RCP8.5, implies more frequent and prolonged heatwaves that will elevate thermal stress in quinoa during its growth and flowering phases, thereby increasing evapotranspiration and the crop's water demand. To adapt, it will be crucial to implement strategies such as efficient irrigation, shading, or the selection of heat-tolerant quinoa varieties to mitigate yield losses and ensure the sustainability of quinoa production under a more extreme climate. The divergence between scenarios highlights the urgency of mitigation actions to reduce severe impacts.

The graphics (**Fig 15A, 15B** and **15C**) for the IPSL, MIROC, and MPI models project a pronounced and consistent increase in maximum temperature, with a critical divergence between scenarios. Under RCP2.6, warming stabilizes after mid-century, whereas under RCP8.5 the increase is accelerated and persistent until 2100, a trend particularly evident

in the MIROC model. This extreme warming implies more intense and frequent heatwaves, which would elevate thermal stress on crops like quinoa, increasing their water demand and the risk of yield losses. The difference between scenarios reinforces the urgent need for mitigation to avoid irreversible impacts on regional agriculture and water resources.

Table 19. Non-parametric test (Sen-Mann-Kendall slope test) for minimum temperature values obtained using the DELTA correction in the IPSL, MIROC, and MPI models, for the period 2006-2100.

Model	S	Z	Sen´s Slope	Significance	Trend
IPSL RCP2.6	22610912	10.495	1.52579E-05	significant	Positive trend at 95%
IPSL RCP8.5	137454608	63.799	0.000155111	significant	Positive trend at 95%
MIROC RCP2.6	43746254	20.305	2.76807E-05	significant	Positive trend at 95%
MIROC RCP8.5	143784589	66.737	0.000156880	significant	Positive trend at 95%
MPI RCP2.6	9656441	4.482	-3.48957E-06	significant	Positive trend at 95%
MPI RCP8.5	128148156	59.480	0.000142089	significant	Positive trend at 95%

The Mann-Kendall test results presented in Table 19 confirm a significant and accelerated warming trend in the maximum temperature for all models (IPSL, MIROC, MPI) and scenarios (RCP2.6 and RCP8.5) in La Molina, with the most intense warming occurring under RCP8.5. This increase implies more frequent, prolonged, and intense heatwaves, which will elevate thermal stress in quinoa during critical stages such as flowering and grain filling, thereby increasing evapotranspiration and water demand. To adapt, it will be crucial to implement strategies such as precision irrigation, shading, or the selection of heat-tolerant quinoa varieties to mitigate yield losses and ensure crop sustainability. The magnitude of warming under RCP8.5 reinforces the urgency of climate mitigation actions.

5. Conclusions

This study assessed climate projections for the 2006-2100 period for quinoa (*Chenopodium quinoa* Willd.) cultivation on the central coast of Peru (Lima) using six coupled models from the CMIP5 project under the RCP2.6 and RCP8.5 scenarios. The results demonstrate a clear divergence in temperature and precipitation projections, which is critically dependent on the emissions trajectory.

Temperature projections show a consistent and accelerated warming, particularly under the high-emissions scenario (RCP8.5). The projected minimum temperature increases by +1.4°C (RCP2.6) to +4.14°C (RCP8.5) by the end of the century, while the maximum temperature increases by +1.2°C and +4.4°C, respectively. These increases are statistically significant (Mann-Kendall test, $p < 0.05$) across all models and periods, indicating a robust warming signal independent of inter-model variability.

Precipitation projections show high uncertainty among models, but key trends were identified. Under RCP2.6, precipitation remains stable or shows slight increases by 2100. Under RCP8.5, greater variability is observed: while models like CNRM-CM5 and MPI-ESM-LR project moderate changes, IPSL-CM5A-MR suggests extreme increases (~5-6 times the historical value) and GFDL-CM3 projects drastic reductions (-66% in the near future). Despite this dispersion, the Mann-Kendall test did not detect significant trends in most models, except for GFDL (positive trend under RCP8.5) and IPSL (significant trends under both scenarios).

The agroclimatic implications are severe under RCP8.5. The rise in minimum temperatures would eliminate frost events, altering crucial vernalization cycles (the process where a plant must experience a period of cold before being able to produce flowers) for crops like quinoa (*Chenopodium quinoa* Willd.), which requires cooling to reproduce. The increase in maximum temperatures and the potential intensification of

droughts (GFDL-CM3) or extreme rainfall (IPSL-CM5A-MR) would increase hydrological and thermal stress, compromising regional agricultural productivity.

The methodological robustness is supported by the use of CMIP5 models, validated with observed data (1975-2005), and statistical analysis using Student's t-tests and the Mann-Kendall test, which confirm the significance of the projected trends. The divergence between scenarios reinforces the urgency of mitigation policies to avoid severe impacts.

This work provides a scientific basis for climate adaptation decision-making in semi-arid coastal regions like Lima, highlighting the need to develop resilient (alternative) crop varieties and efficient water management systems for the coasts of Peru.

Acknowledgements ‘‘The authors acknowledge the kind support of the research program of Native Cereals and Grains of UNALM to the Experimental Irrigation Area (AER) of UNALM and the research group Remote sensing and climate change applied to water resources and agricultura.

References

1. Ocampo, O. (2011). El cambio climático y su impacto en el agro. *Revista de ingeniería*, (33), 115-123. http://www.scielo.org.co/scielo.php?pid=S0121-49932011000100012&script=sci_arttext
2. Mello, C. R., Ávila, L. F., Viola, M. R., Curi, N., & Darrel, N. Ll. (2015). Assessing the climate change impacts on the rainfall erosivity throughout the twenty-first century in the Grande River Basin (GRB) headwaters, Southeastern Brazil. *Environmental Earth Sciences*, *73*(12), 8683-8698. https://link.springer.com/article/10.1007/s12665-015-4033-3
3. Thomas, D. S. G., Twyman, Ch., Osbahr, H. & Hewitson, B. (2011). Adaptation to climate change and variability: farmer responses to intra-seasonal precipitation

trends in South Africa. En C. Williams & D. Kniveton (Eds.), *African Climate and Climate Change. Advances in Global Change Research* (vol. 43, pp. 155-178). Springer. https://doi.org/10.1007/978-90-481-3842-5_7

4. Chaudhary, D. P., Jat, S. L., Kumar, R., Kumar, A., & Kumar, B. (2013). Fodder quality of maize: Its preservation. In *Maize: Nutrition dynamics and novel uses* (pp. 153-160). New Delhi: Springer India. https://link.springer.com/chapter/10.1007/978-81-322-1623-0_13
5. Jain, T. B., Pilliod, D. S., Graham, R. T., Lentile, L. B., & Sandquist, J. E. (2012). Index for characterizing post-fire soil environments in temperate coniferous forests. *Forests*, *3*, 445-466. https://doi.org/10.3390/f3030445
6. Kumar, M., Bhatt, V. P., & Rajwar, G. S. (2006). Plant and soil diversities in a sub tropical forest of the Garhwal Himalaya. *Ghana Journal of Forestry*, *19-20*, 1-19.
7. Kumar, V., & Ladha, J. K. (2011). Chapter six. Direct seeding of rice: recent developments and future research needs. En *Advances in agronomy* (vol. 111, pp. 297-413). Elsevier. http://dx.doi.org/10.1016/B978-0-12-387689-8.00001-1.
8. Ravindranath, N., Rao, S., Sharma, N., Nair, M., Gopalakrishnan, R., Rao, A., Malaviya, S., Tiwari, R., Sagadevan, A., Munsi, M., Krishna, N., & Govindasamy, B. (2011). Climate change vulnerability profiles for North East India. *Current Science*, *101*, 384-394. https://www.jstor.org/stable/24078517
9. Sharmila, S., Joseph, S., Sahai, A. K., Abhilash, S., & Chattopadhyay, R. (2015). Future projection of Indian summer monsoon variability under climate change scenario: an assessment from CMIP5 climate models. *Global and Planetary Change*, *124*, 62-78. https://doi.org/10.1016/j.gloplacha.2014.11.004

10. Muñoz, V. E. G. (2024). Estado del arte sobre modelos de circulación global para resistir el problema del cambio climático. *Revista Torreón Universitario*, *13*(36), 6-17. https://doi.org/10.5377/rtu.v13i36.17630

11. Poveda, G., Espinoza, J. C., Zuluaga, M. D., Solman, S. A., Garreaud, R., & Van Oevelen, P. J. (2020). High impact weather events in the Andes. *Frontiers in Earth Science*, *8*, 162. https://doi.org/10.3389/feart.2020.00162

12. Taylor, K. E., Stouffer, R. J., & Meehl, G. A. (2012). An overview of CMIP5 and the experiment design. *Bulletin of the American Meteorological Society*, *93*(4), 485–498. https://doi.org/10.1175/BAMS-D-11-00094.1

13. Eyring, V., Bony, S., Meehl, G. A., Senior, C. A., Stevens, B., Stouffer, R. J., & Taylor, K. E. (2016). *Overview of the Coupled Model Intercomparison Project Phase 6 (CMIP6) experimental design and organization*. Geoscientific Model Development, 9(5), 1937–1958. https://doi.org/10.5194/gmd-9-1937-2016

14. Kuma, P., Bender, F. A. M., & Jönsson, A. R. (2023). Climate model code genealogy and its relation to climate feedbacks and sensitivity. *Journal of Advances in Modeling Earth Systems*, *15*(7), e2022MS003588. https://doi.org/10.1029/2022MS003588

15. Brunet, M., Saladié, O., Jones, P., Sigró, J., Aguilar, E., Moberg, A., Lister, D., Walther, A. M., Lopez, D., & Almarza, C. (2006). The development of a new dataset of Spanish daily adjusted temperature series (SDATS) (1850-2003). *International Journal of Climatology*, *26*, 1777-1802. DOI: 10.1002/joc.1338. http://www.c3.urv.cat/docs/publicacions/2006/PDF_23_Development_new_dataset.pdf

16. Montaño-Roldan, V. L., Caicedo, P. L. O., Vega, A. A. G., Vélez, C. E. Á., & Tambaco, A. J. C. (2023). El cambio climático y sus efectos en la biodiversidad en

Perú. Ibero-American Journal of Engineering & Technology Studies, 3(2), 34-42. https://doi.org/10.56183/iberotecs.v3i2.630

17. Nagy, G. J., Gutiérrez, O., Brugnoli, E., Verocai, J. E., Gómez-Erache, M., Villamizar, A., ... & Amaro, N. (2019). Climate vulnerability, impacts and adaptation in Central and South America coastal areas. Regional Studies in Marine Science, 29, 100683. https://doi.org/10.1016/j.rsma.2019.100683
18. Weigel, K., Bock, L., Gier, B. K., Lauer, A., Righi, M., Schlund, M., ... & Eyring, V. (2020). Earth System Model Evaluation Tool (ESMValTool) v2. 0–diagnostics for extreme events, regional and impact evaluation and analysis of Earth system models in CMIP. *Geoscientific Model Development Discussions*, *2020*, 1-43. https://doi.org/10.5194/gmd-14-3159-2021
19. Ortega, G., Arias, P. A., Villegas, J. C., Marquet, P. A., & Nobre, P. (2021). Present-day and future climate over central and South America according to CMIP5/CMIP6 models. *International Journal of Climatology*, *41*(15), 6713-6735. https://doi.org/10.1002/joc.7221
20. IPCC. (2021). *Sixth Assessment Report: Climate Change 2021 - The Physical Science Basis*. Cambridge University Press. https://www.ipcc.ch/report/ar6/wg1/
21. Evans, J. P., Bormann, K., Katzfey, J., Dean, S., & Arritt, R. (2016). Regional climate model projections of the South Pacific Convergence Zone. *Climate dynamics*, *47*(3), 817-829. https://link.springer.com/article/10.1007/s00382-015-2873-x
22. MINAM (Ministerio del Ambiente del Perú). (2019). *Plan Nacional de Adaptación al Cambio Climático*. Lima: MINAM. https://sinia.minam.gob.pe/sites/default/files/siar-puno/archivos/public/docs/nap_planeamiento_e_implementacion_gore.pdf

23. Moss, R. H., Edmonds, J. A., Hibbard, K. A., Manning, M. R., Rose, S. K., Van Vuuren, D. P., Carter, T. R., Emori, S., Kainuma, M., Kram, T., Meehl, G. A., Mitchell, J. F. B., Nakicenovic, N., Riahi, K., Smith, S. J., Stouffer, R. J., Thomson, A. M., Weyant, J. P., & Wilbanks, T. J. (2010). The next generation of scenarios for climate change research and assessment. *Nature*, *463*(7282), 747-756. http://dx.doi.org/10.1038/ nature08823 https://www.nature.com/articles/nature08823

24. Lucatero, D., Madsen, H., Refsgaard, J. C., Kidmose, J., & Jensen, K. H. (2018). On the skill of raw and post-processed ensemble seasonal meteorological forecasts in Denmark. *Hydrology and Earth System Sciences*, *22*(12), 6591-6609. https://doi.org/10.5194/hess-22-6591-2018

25. García López, Y. J., Bedón Monzón, H. M., & Durán Gómez, M. (2022). Proyección climática para el periodo 2006-2075 para el valle de Jauja, simulada por la intercomparación de modelos acoplados CSIRO Mk 3.0, MIROC-ESM y CNRM de fase 5 (CMIP5). https://doi.org/10.26439/ing.ind2022.n.5813

26. Mendoza-Márquez, B., Chuchon-Remon, R., Ramos-Fernández, L., Falconí-Palomino, J., Garcia-Lopez, Y., & Gómez-Pando, L. (2025). Water Stress Thresholds and Irrigation Management Via Infrared Thermography and AquaCrop Model in Quinoa Cultivation in Arid Zones. *Agricultural Research*, 1-11. https://doi.org/10.1007/s40003-025-00869-0

27. Teutschbein, C. and Seibert, J.: Bias correction of regional climate model simulations for hydrological climate-change impact studies: Review and evaluation of different methods, J. Hydrol., 456– 457, 12–29. https://doi.org/10.1016/j.jhydrol.2012.05.052

28. Wetterhall, F., Winsemius, H. C., Dutra, E., Werner, M., & Pappenberger, E. (2015). Seasonal predictions of agro-meteorological drought indicators for the Limpopo

basin.*Hydrology and Earth System Sciences*, *19*(6), 2577-2586. https://doi.org/10.5194/hess-19-2577-2015

29. Lenderink, G., Buishand, A., & Van Deursen, W. (2007). Estimates of future discharges of the river Rhine using two scenario methodologies: direct versus delta approach. *Hydrology and Earth System Sciences*, *11*(3), 1145-1159. https://doi.org/10.5194/hess-11-1145-2007
30. Fang, G. H., Yang, J., Chen, Y. N., & Zammit, C. (2015). Comparing bias correction methods in downscaling meteorological variables for a hydrologic impact study in an arid area in China. *Hydrology and Earth System Sciences*, *19*(6), 2547-2559. https://doi.org/10.5194/hess-19-2547-2015
31. Eisner, S., Voss, F., & Kynast, E. (2012). Statistical bias correction of global climate projections–consequences for large scale modeling of flood flows. *Advances in Geosciences*, *31*, 75-82. https://doi.org/10.5194/adgeo-31-75-2012
32. Wild, M., Folini, D., Schär, C., Loeb, N., Dutton, E. G., & König-Langlo, G. (2013). The global energy balance from a surface perspective. *Climate Dynamics*, *40*(11-12), 3107-3134. https://link.springer.com/article/10.1007/s00382-012-1569-8
33. IPCC. (2014). Informe de síntesis. Contribución de los Grupos de trabajo I, II y III al Quinto Informe de Evaluación del Grupo Intergubernamental de Expertos sobre el Cambio Climático [Equipo principal de redacción, R.K. Pachauri y L.A. Meyer (eds.)]. Ginebra, Suiza, 157p. https://www.ipcc.ch/site/assets/uploads/2018/02/SYR_AR5_FINAL_full_es.pdf
34. SENAMHI. (2023). *Base de datos meteorológicos históricos*. Servicio Nacional de Meteorología e Hidrología del Perú. https://www.senamhi.gob.pe/servicios/?p=estaciones

35. Peel, M. C., Finlayson, B. L., & McMahon, T. A. (2007). Updated world map of the Köppen-Geiger climate classification. *Hydrology and Earth System Sciences*, *11*(5), 1633–1644. https://doi.org/10.5194/hess-11-1633-2007.

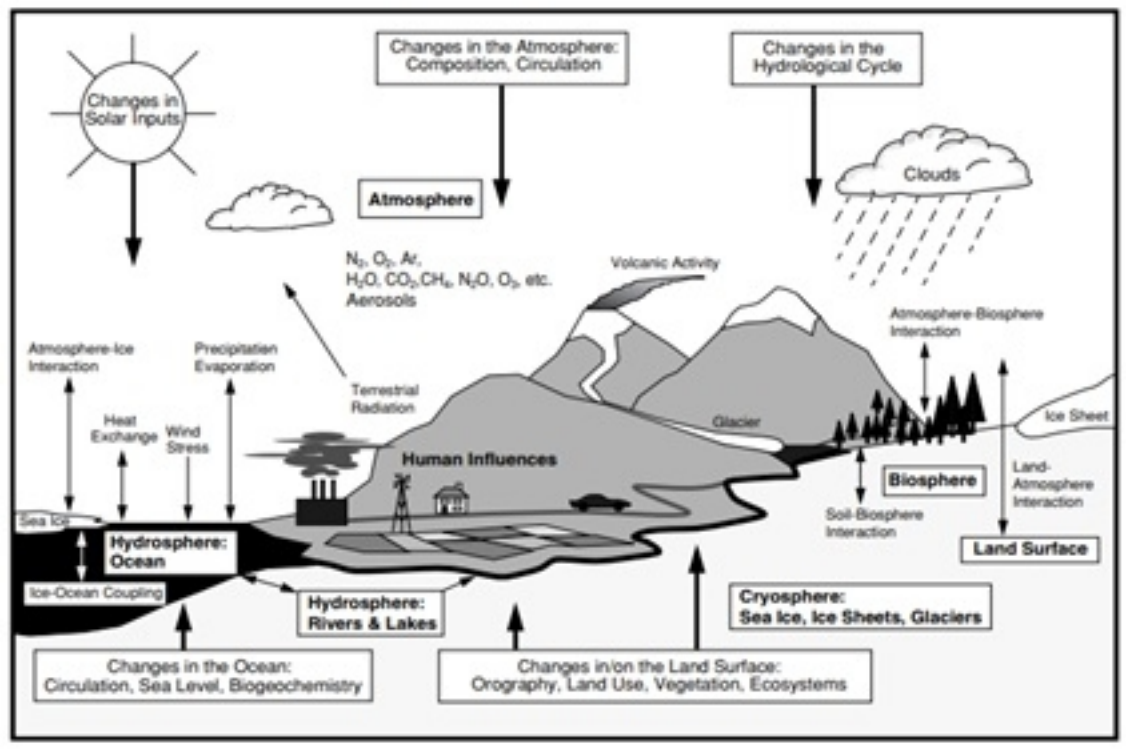
Changes in Solar Inputs
Changes in the Atmosphere: Composition, Circulation
Changes in the Hydrological Cycle
Atmosphere
Clouds
N_2, O_2, Ar,
H_2O, CO_2, CH_4, N_2O, O_3, etc.
Aerosols
Volcanic Activity
Atmosphere-Ice Interaction
Precipitation Evaporation
Terrestrial Radiation
Heat Exchange
Wind Stress
Glacier
Atmosphere-Biosphere Interaction
Ice Sheet
Human Influences
Biosphere
Land-Atmosphere Interaction
Sea Ice
Soil-Biosphere Interaction
Hydrosphere: Ocean
Land Surface
Ice-Ocean Coupling
Hydrosphere: Rivers & Lakes
Cryosphere: Sea Ice, Ice Sheets, Glaciers
Changes in the Ocean: Circulation, Sea Level, Biogeochemistry
Changes in/on the Land Surface: Orography, Land Use, Vegetation, Ecosystems


El Agustino
Santa Anita
Real Plaza Puruchuco
Estadio Monumental «U»
Circuito Mágico del Agua
Parque de Los Anillos
Jockey Plaza
Wong La Planicie
La Molina
Toros de Cieneguilla
Universidad Peruana de Ciencias Aplicadas
San Borja
Museo de Sitio Pucllana
Surquillo
Miraflores
Santiago de Surco
Plaza central de Manchay-Pachacamac
Apu Siqay
Lomas del Paraiso
Barranco
Datos del mapa ©2025 Google


Av. La Universidad
Av. La Universidad
Jardín Botánico
Calle Mocan
Universidad Agraria de La Molina

Cumulative Precipitation (mm)

Historical BaseLine and Projected Annual Precipitation (RCP2.6 Scenario)

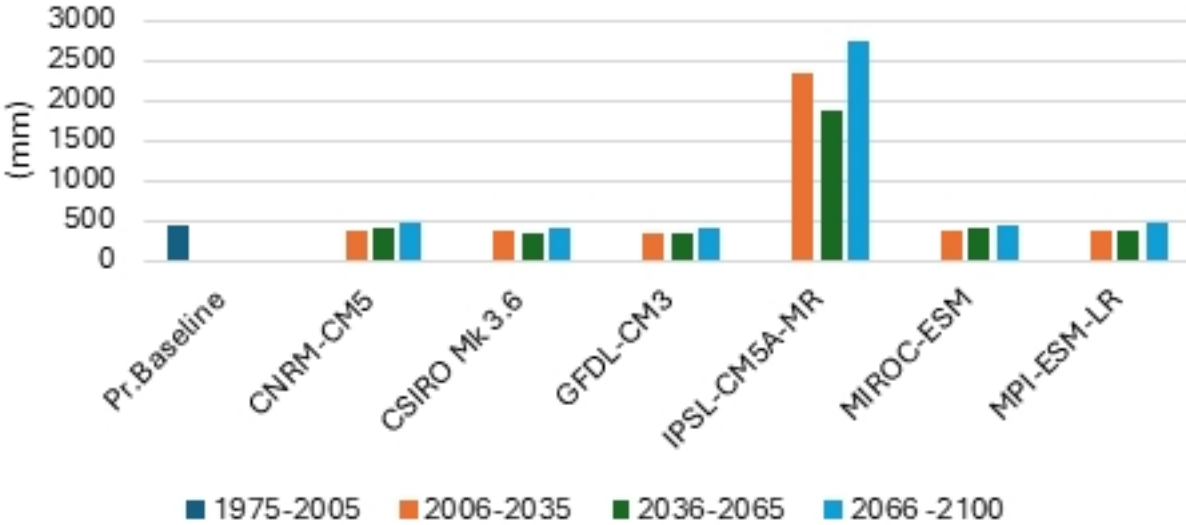

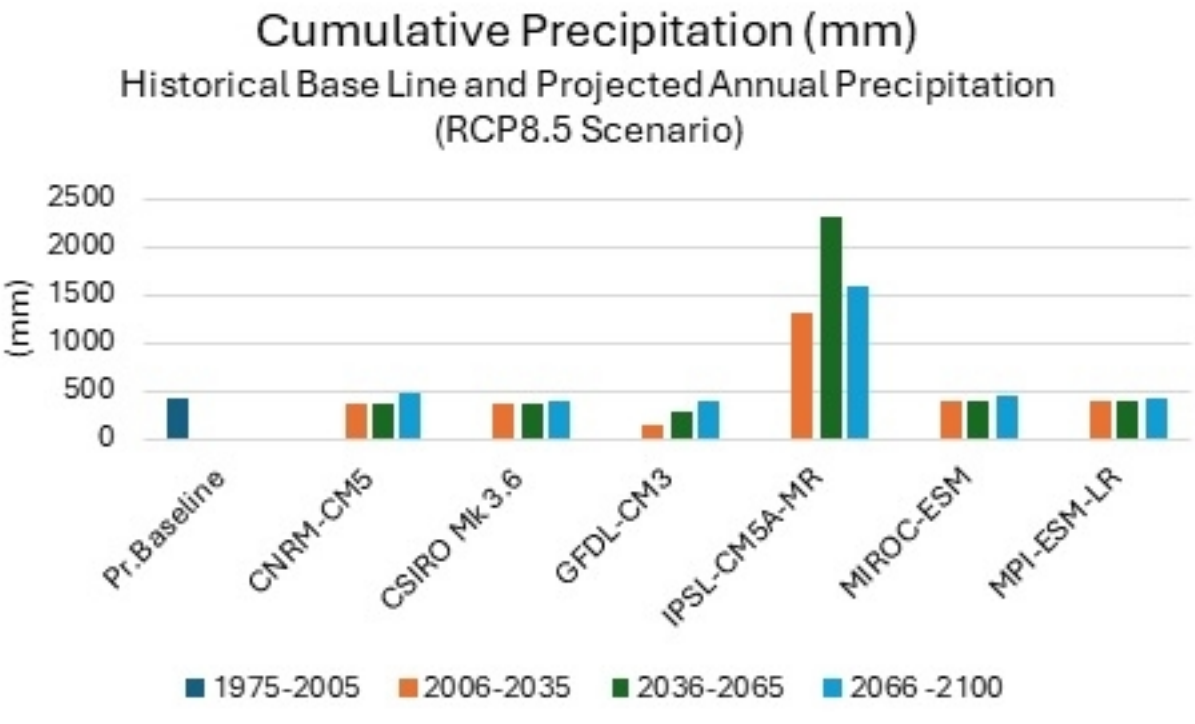
Cumulative Precipitation (mm)
Historical Base Line and Projected Annual Precipitation
(RCP8.5 Scenario)
2500
2000
1500
1000
500
0
(mm)
Pr.Baseline
CNRM-CM5
CSIRO Mk 3.6
GFDL-CM3
IPSL-CM5A-MR
MIROC-ESM
MPI-ESM-LR
1975-2005
2006-2035
2036-2065
2066 -2100

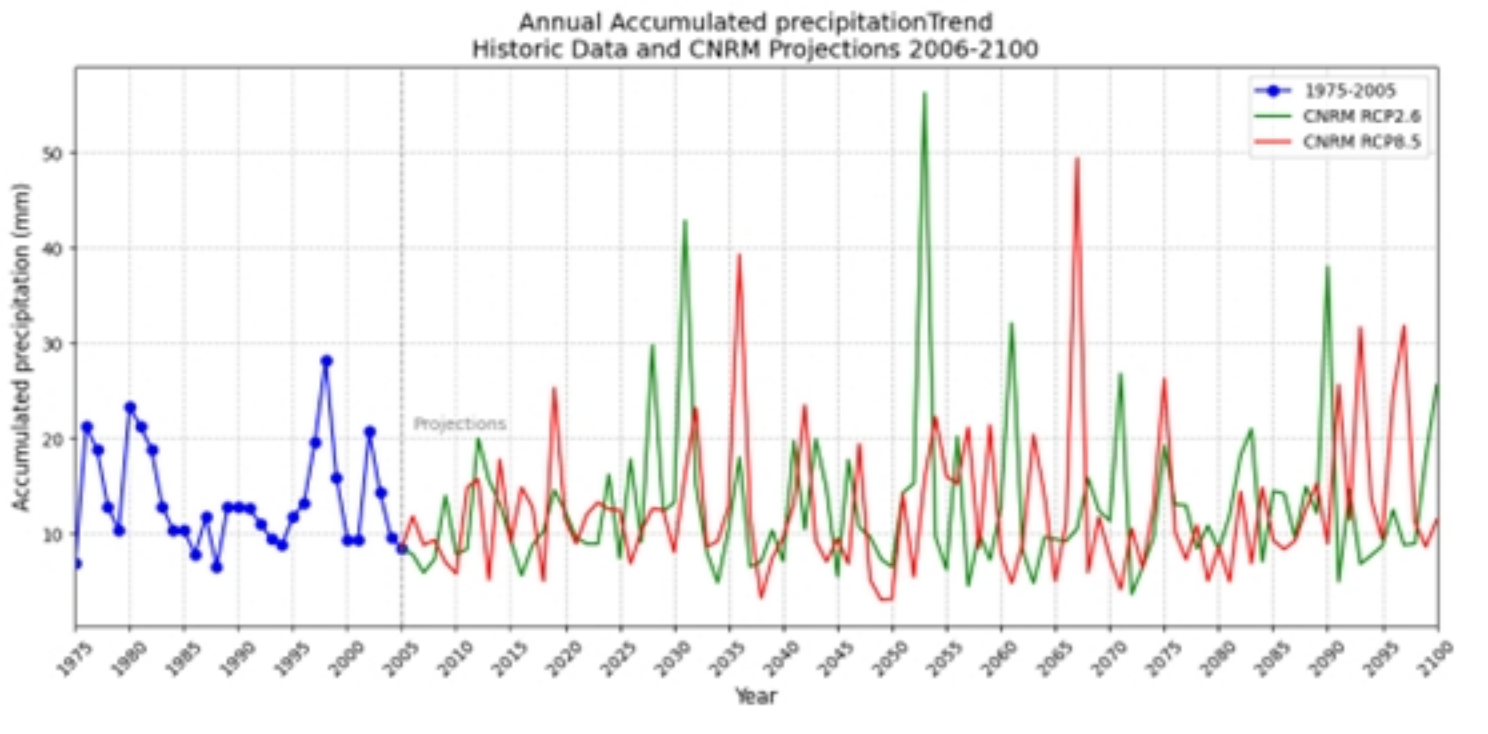
Annual Accumulated precipitationTrend
Historic Data and CNRM Projections 2006-2100
1975-2005
CNRM RCP2.6
CNRM RCP8.5
Projections
Accumulated precipitation (mm)
Year

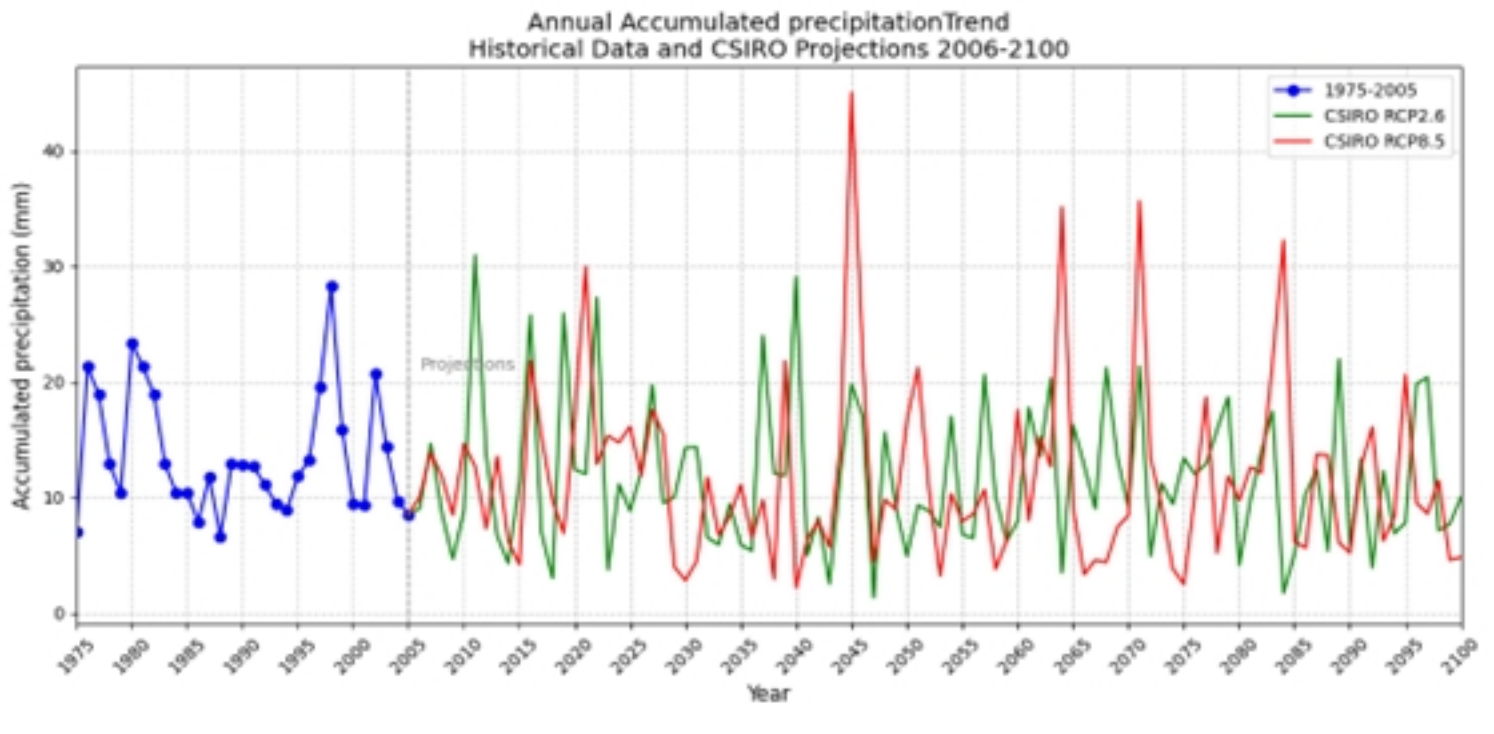
Annual Accumulated precipitationTrend
Historical Data and CSIRO Projections 2006-2100
1975-2005
CSIRO RCP2.6
CSIRO RCP8.5
Projections
Accumulated precipitation (mm)
Year
0
10
20
30
40
1975
1980
1985
1990
1995
2000
2005
2010
2015
2020
2025
2030
2035
2040
2045
2050
2055
2060
2065
2070
2075
2080
2085
2090
2095
2100

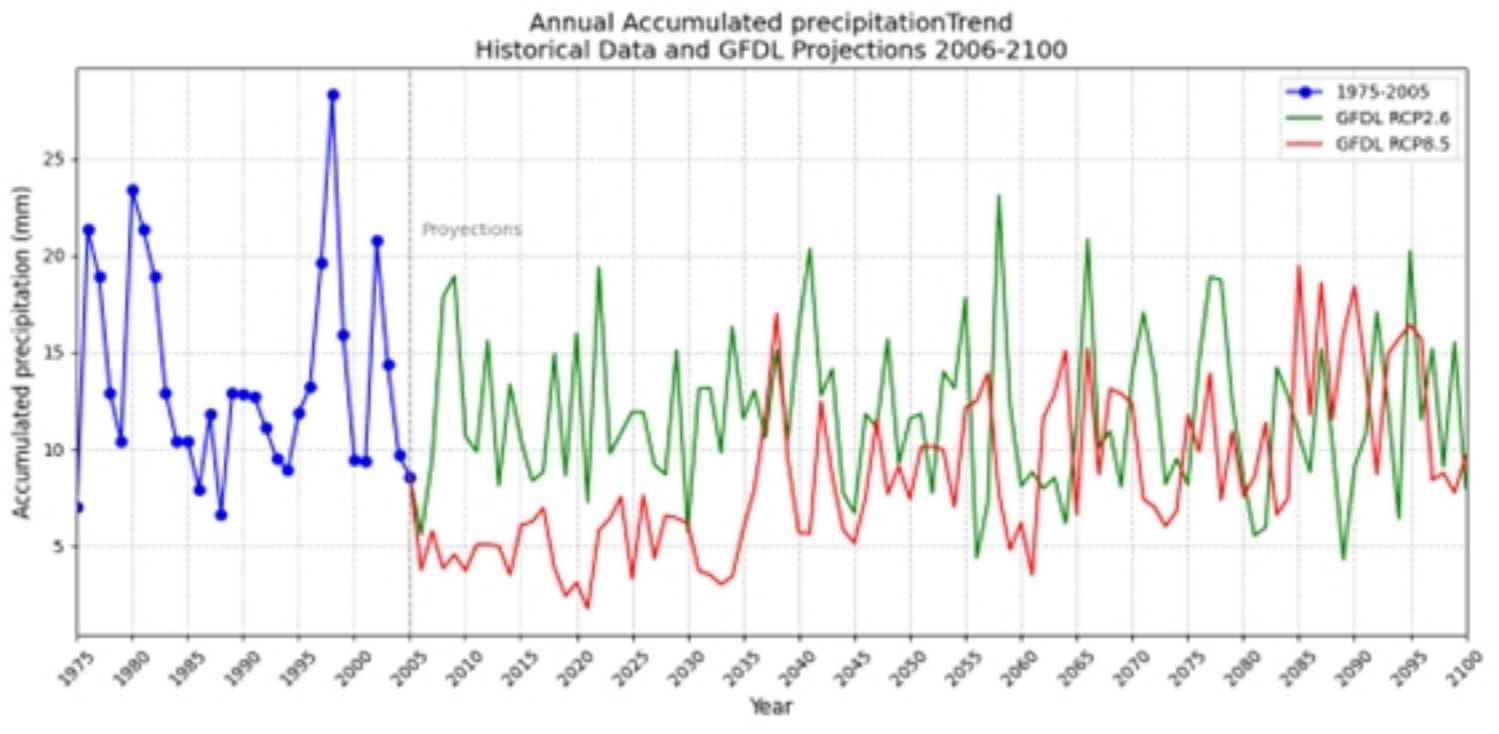
Annual Accumulated precipitationTrend
Historical Data and GFDL Projections 2006-2100
1975-2005
GFDL RCP2.6
GFDL RCP8.5
Proyections
Accumulated precipitation (mm)
Year

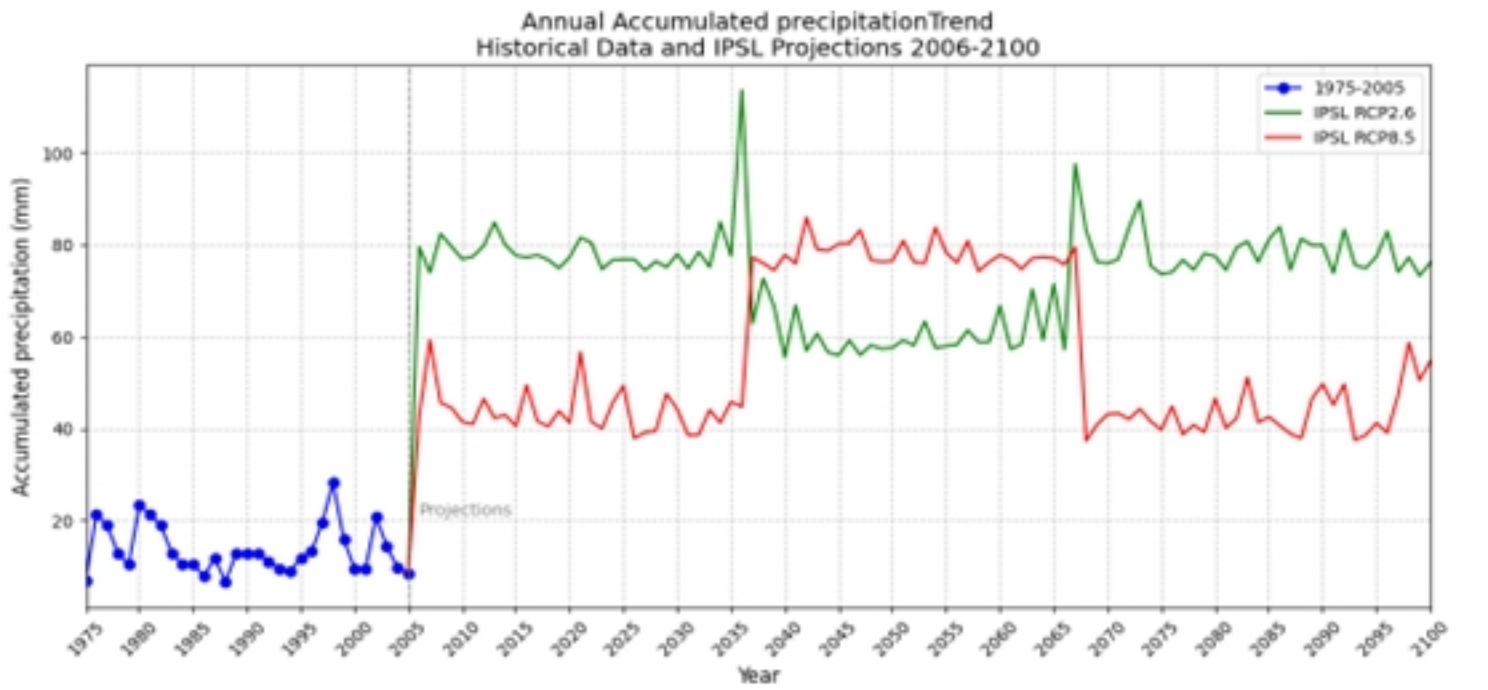
Annual Accumulated precipitationTrend
Historical Data and IPSL Projections 2006-2100
1975-2005
IPSL RCP2.6
IPSL RCP8.5
Projections
Accumulated precipitation (mm)
Year
20
40
60
80
100
1975
1980
1985
1990
1995
2000
2005
2010
2015
2020
2025
2030
2035
2040
2045
2050
2055
2060
2065
2070
2075
2080
2085
2090
2095
2100

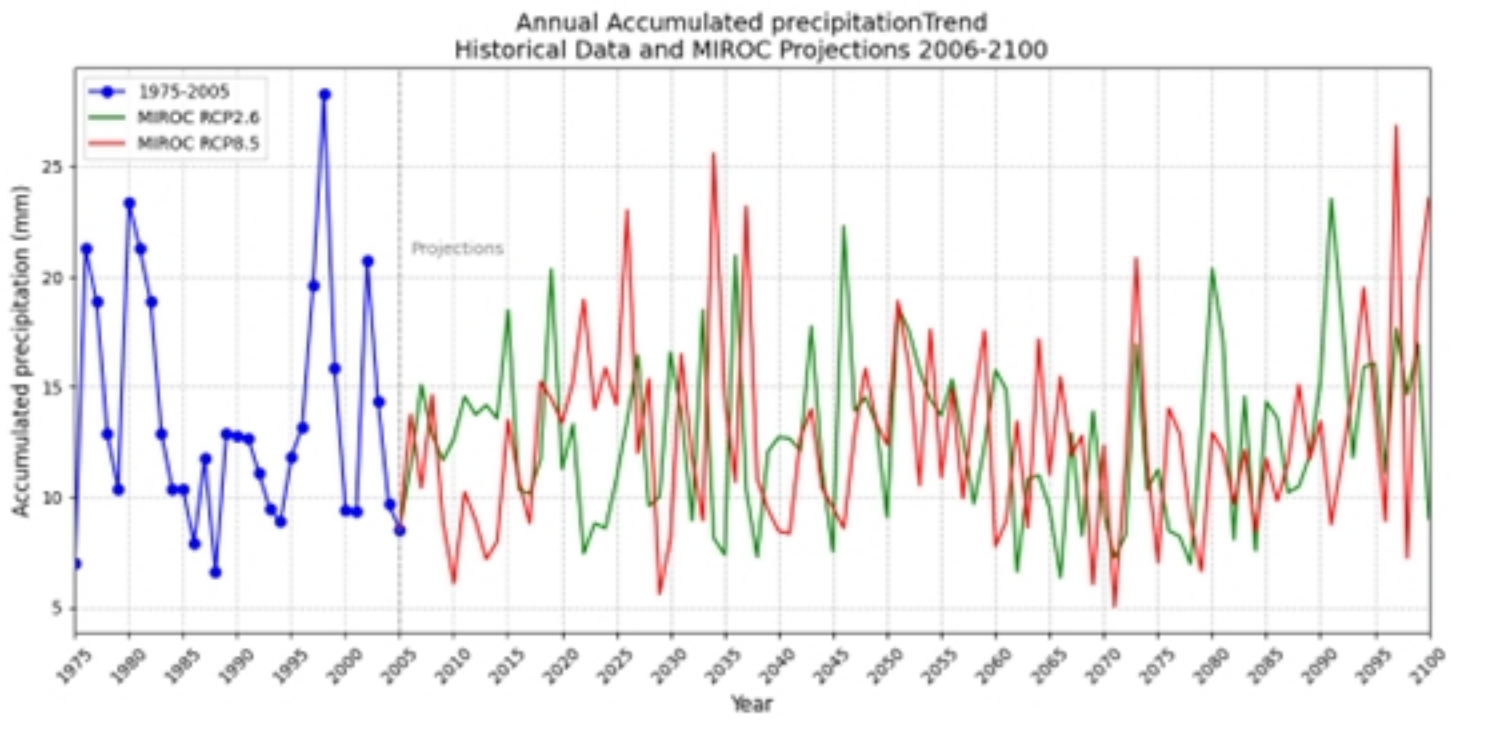
Annual Accumulated precipitationTrend
Historical Data and MIROC Projections 2006-2100
1975-2005
MIROC RCP2.6
MIROC RCP8.5
Projections
Accumulated precipitation (mm)
Year

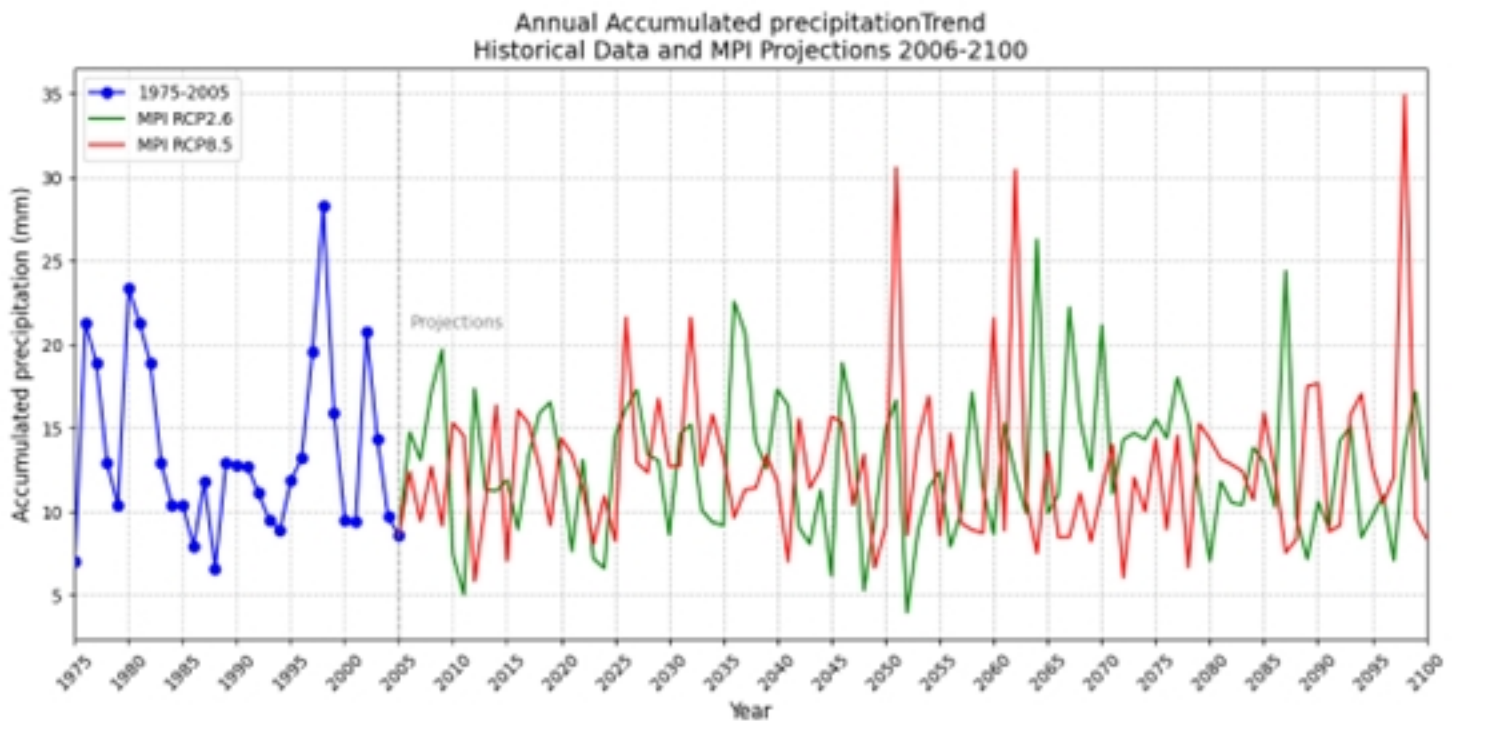
Annual Accumulated precipitationTrend
Historical Data and MPI Projections 2006-2100
1975-2005
MPI RCP2.6
MPI RCP8.5
Projections
Accumulated precipitation (mm)
Year

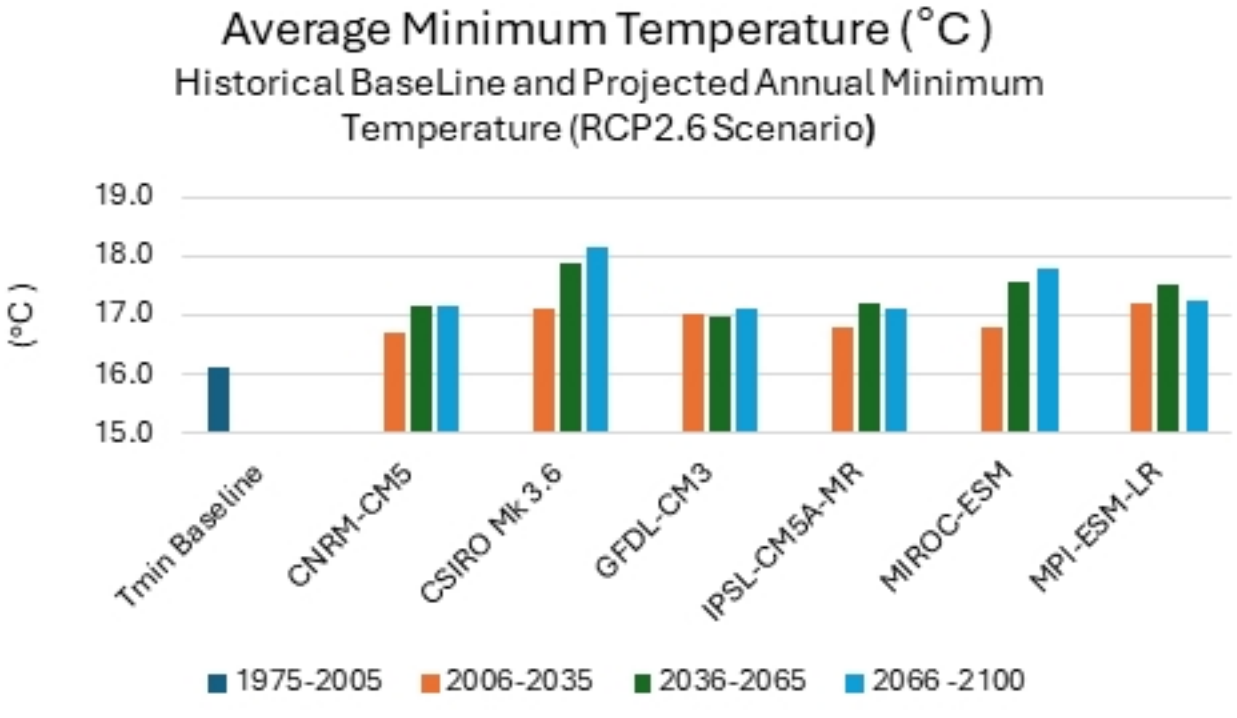
Average Minimum Temperature (°C)
Historical BaseLine and Projected Annual Minimum Temperature (RCP2.6 Scenario)
(°C)
19.0
18.0
17.0
16.0
15.0
Tmin Baseline
CNRM-CM5
CSIRO Mk 3.6
GFDL-CM3
IPSL-CM5A-MR
MIROC-ESM
MPI-ESM-LR
1975-2005
2006-2035
2036-2065
2066 -2100

Average Minimum Temperature (°C)

Historical BaseLine and Projected Annual Minimum Temperature (RCP8.5 Scenario)

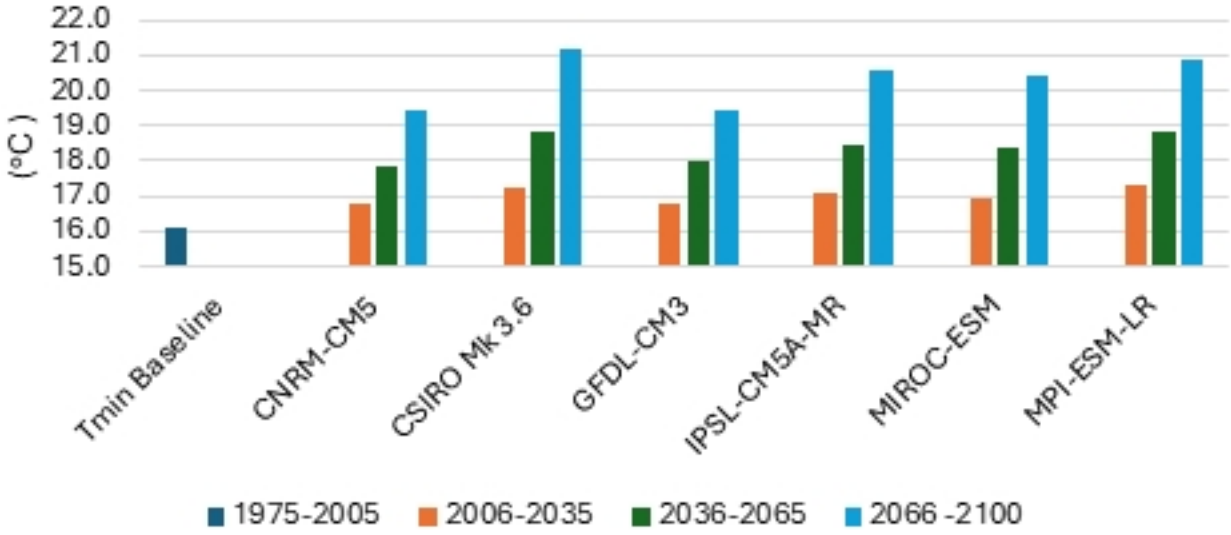

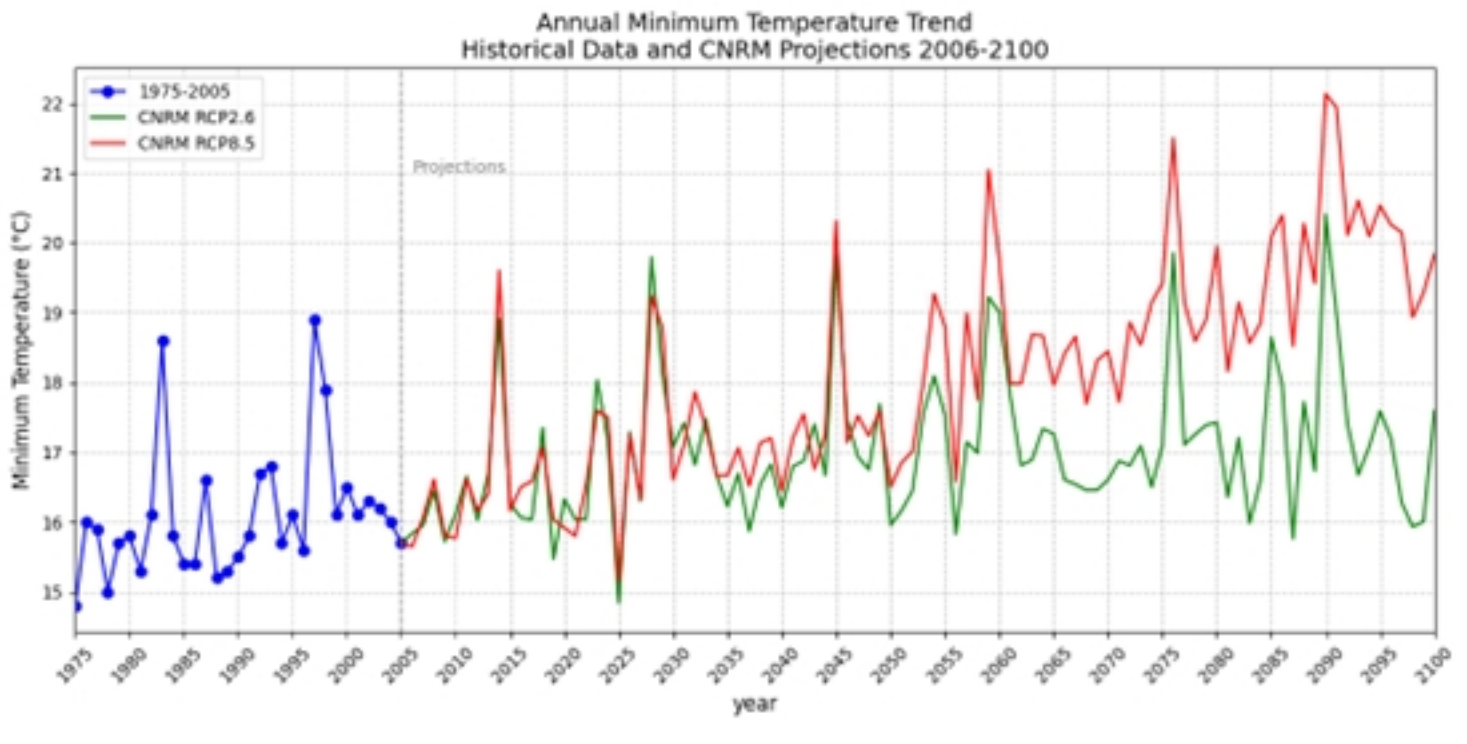
Annual Minimum Temperature Trend
Historical Data and CNRM Projections 2006-2100
1975-2005
CNRM RCP2.6
CNRM RCP8.5
Projections
Minimum Temperature (°C)
year

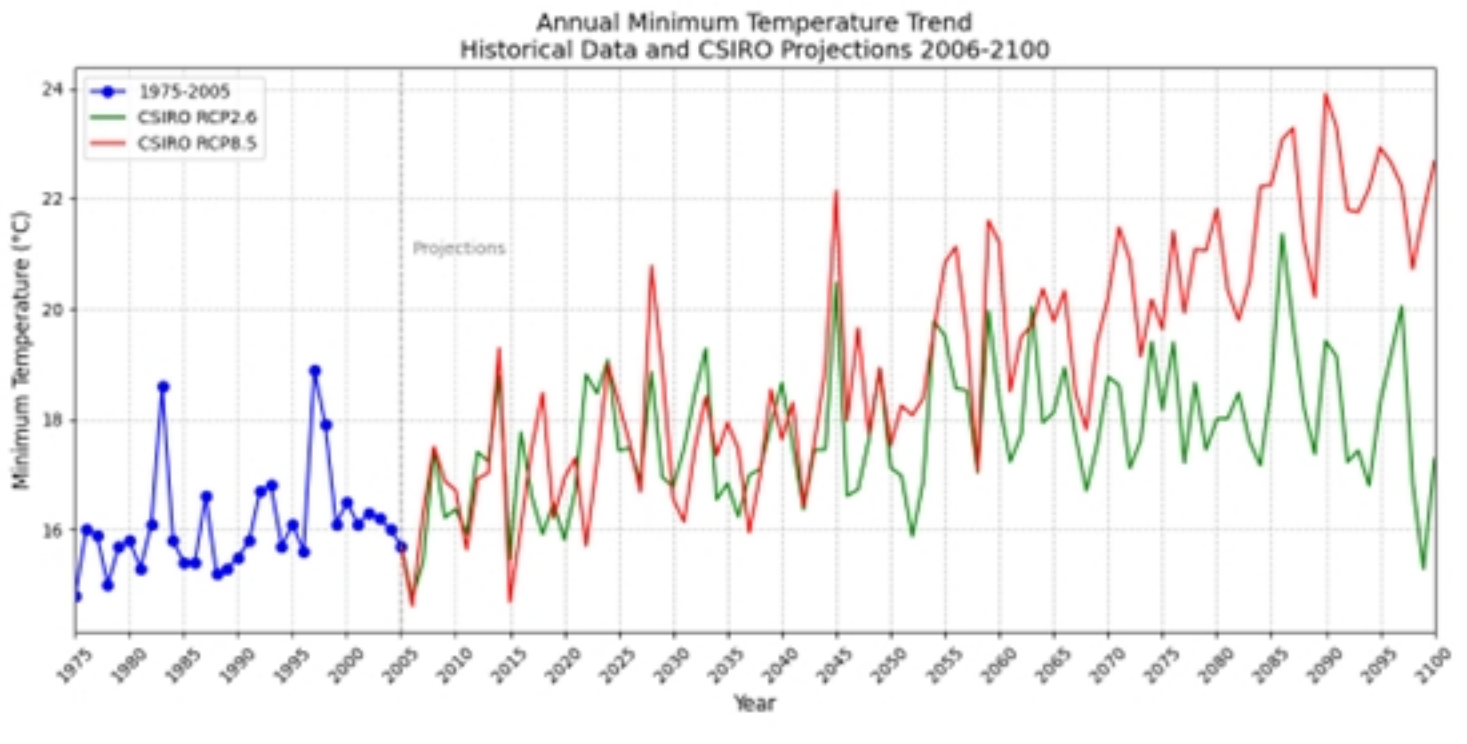
Annual Minimum Temperature Trend
Historical Data and CSIRO Projections 2006-2100
1975-2005
CSIRO RCP2.6
CSIRO RCP8.5
Projections
Minimum Temperature (°C)
Year
24
22
20
18
16
1975
1980
1985
1990
1995
2000
2005
2010
2015
2020
2025
2030
2035
2040
2045
2050
2055
2060
2065
2070
2075
2080
2085
2090
2095
2100

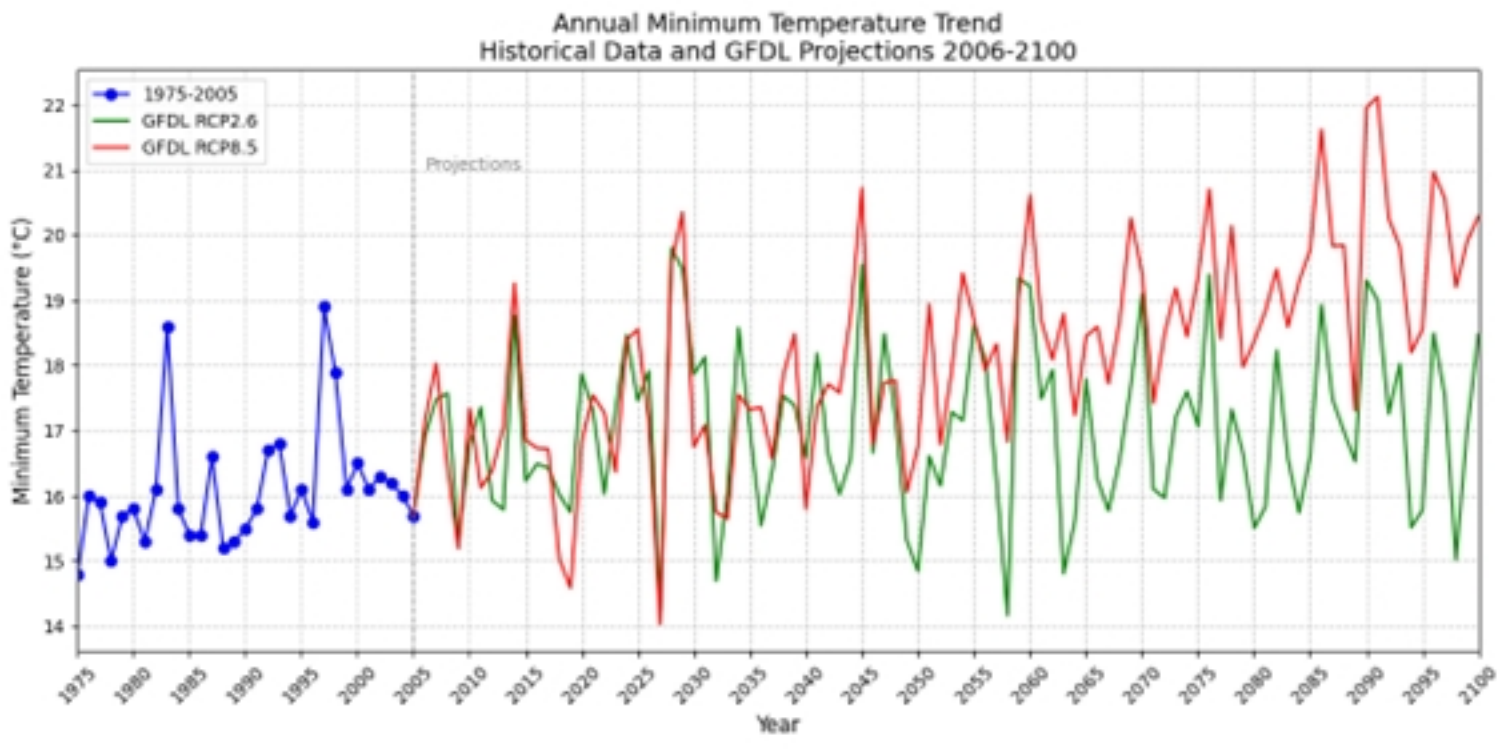
Annual Minimum Temperature Trend
Historical Data and GFDL Projections 2006-2100
1975-2005
GFDL RCP2.6
GFDL RCP8.5
Projections
Minimum Temperature (°C)
Year

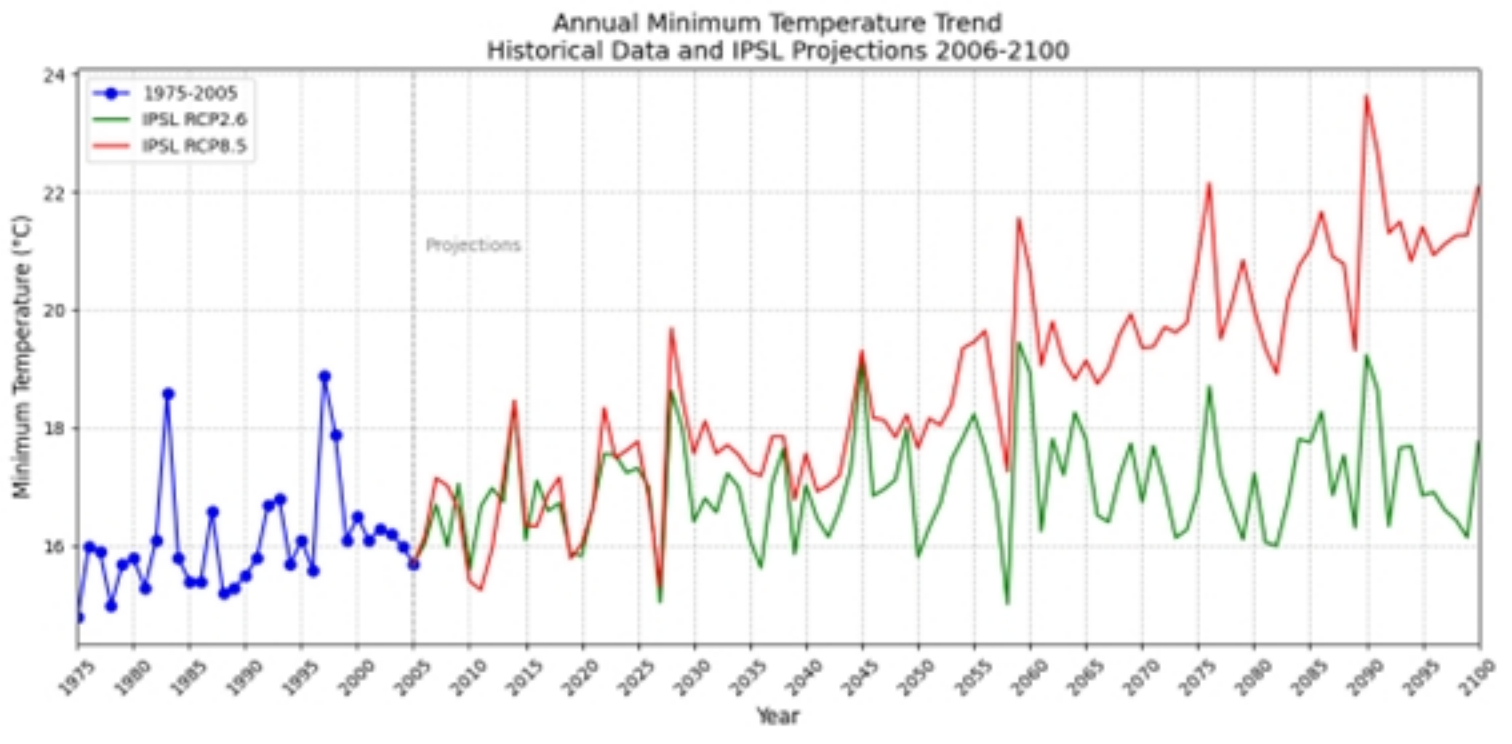
Annual Minimum Temperature Trend
Historical Data and IPSL Projections 2006-2100
1975-2005
IPSL RCP2.6
IPSL RCP8.5
Projections
Minimum Temperature (°C)
Year
24
22
20
18
16
1975
1980
1985
1990
1995
2000
2005
2010
2015
2020
2025
2030
2035
2040
2045
2050
2055
2060
2065
2070
2075
2080
2085
2090
2095
2100

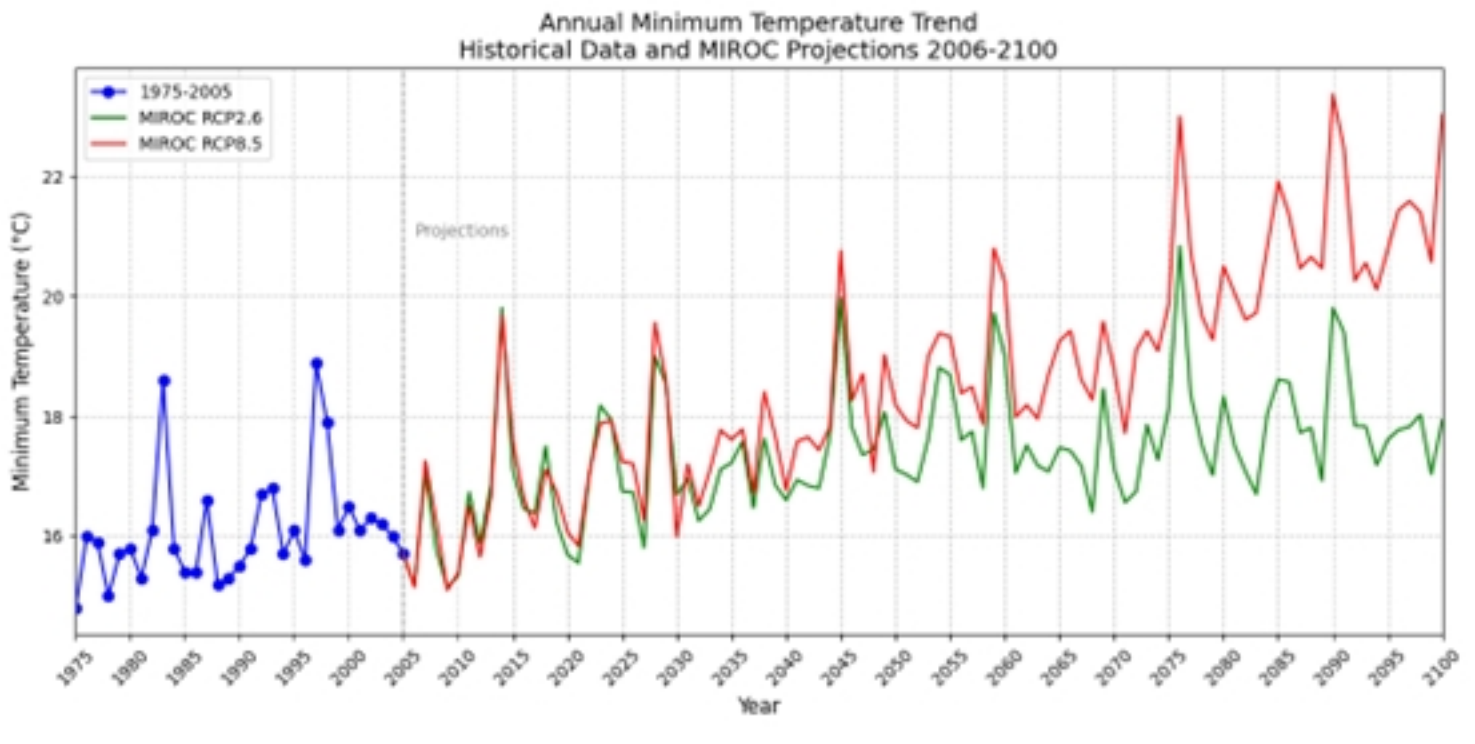
Annual Minimum Temperature Trend
Historical Data and MIROC Projections 2006-2100
1975-2005
MIROC RCP2.6
MIROC RCP8.5
Projections
Minimum Temperature (°C)
Year

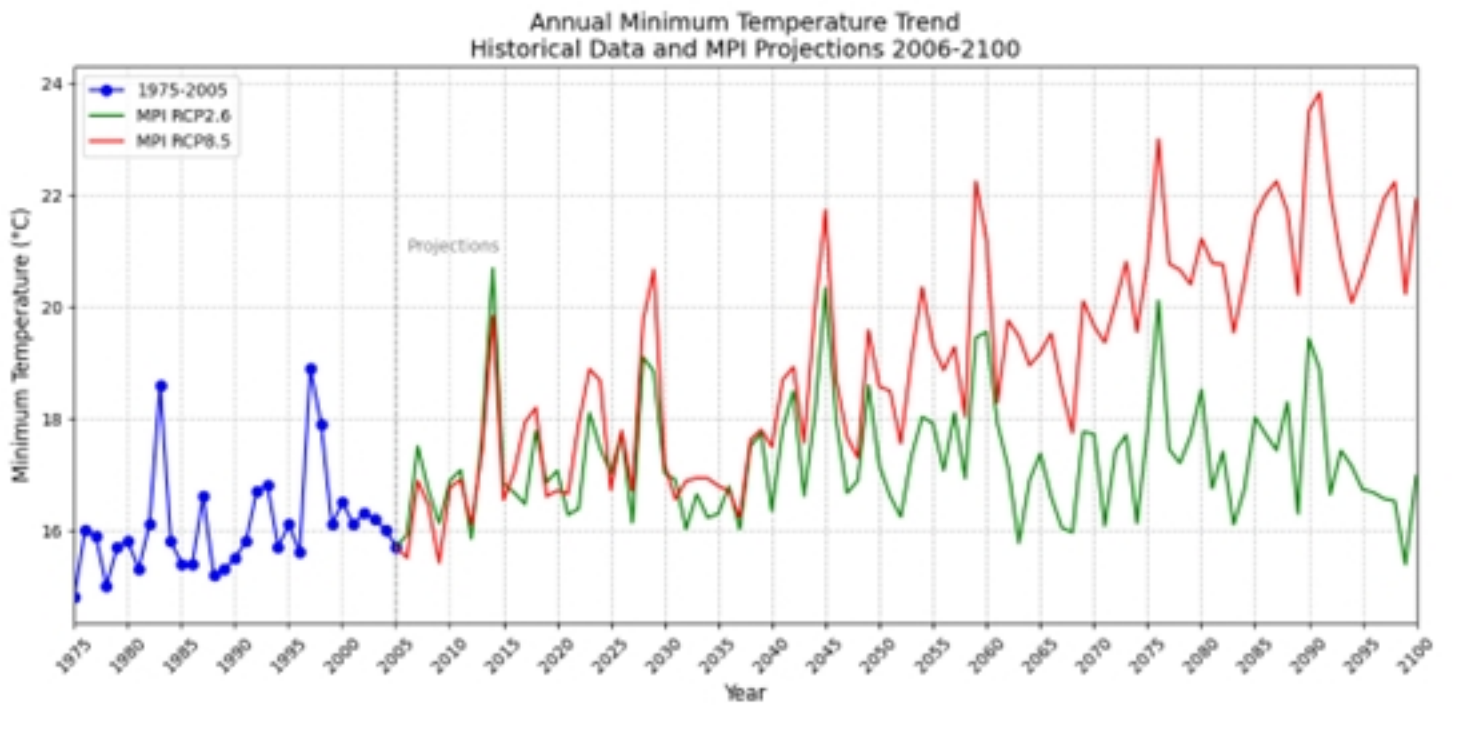
Annual Minimum Temperature Trend
Historical Data and MPI Projections 2006-2100
1975-2005
MPI RCP2.6
MPI RCP8.5
Projections
Minimum Temperature (°C)
Year
16
18
20
22
24
1975
1980
1985
1990
1995
2000
2005
2010
2015
2020
2025
2030
2035
2040
2045
2050
2055
2060
2065
2070
2075
2080
2085
2090
2095
2100

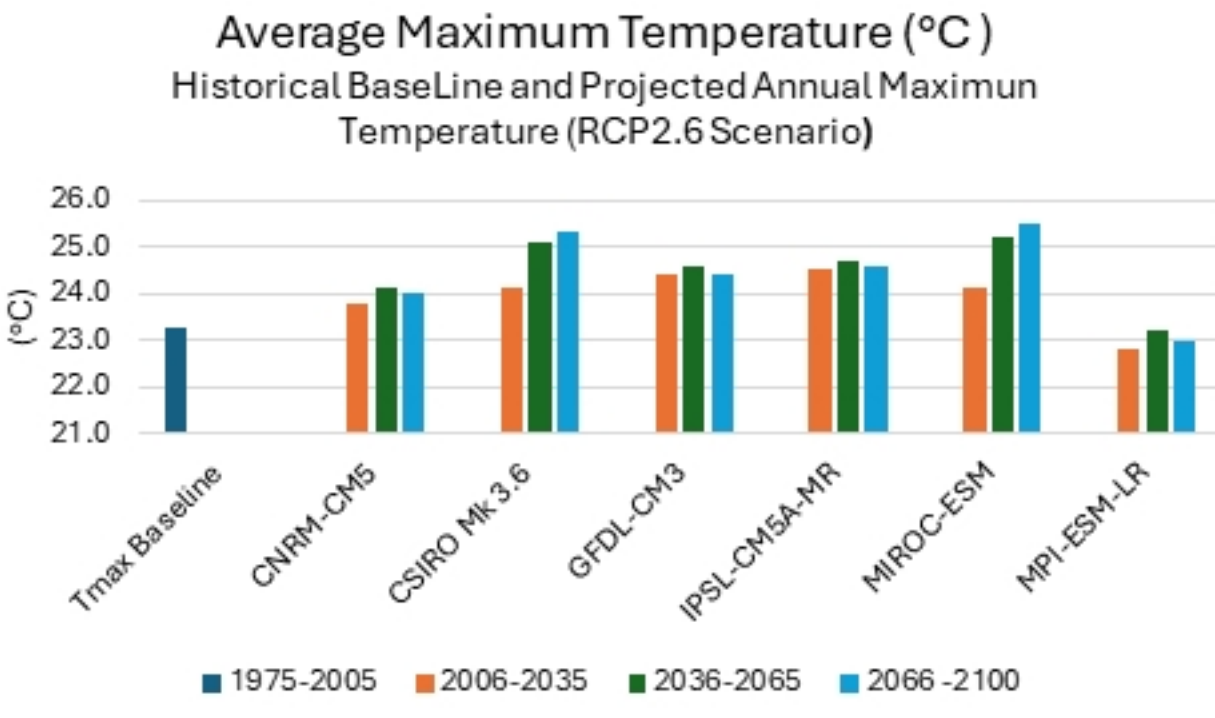
Average Maximum Temperature (°C)
Historical BaseLine and Projected Annual Maximun Temperature (RCP2.6 Scenario)
(°C)
26.0
25.0
24.0
23.0
22.0
21.0
Tmax Baseline
CNRM-CM5
CSIRO Mk 3.6
GFDL-CM3
IPSL-CM5A-MR
MIROC-ESM
MPI-ESM-LR
1975-2005
2006-2035
2036-2065
2066 -2100

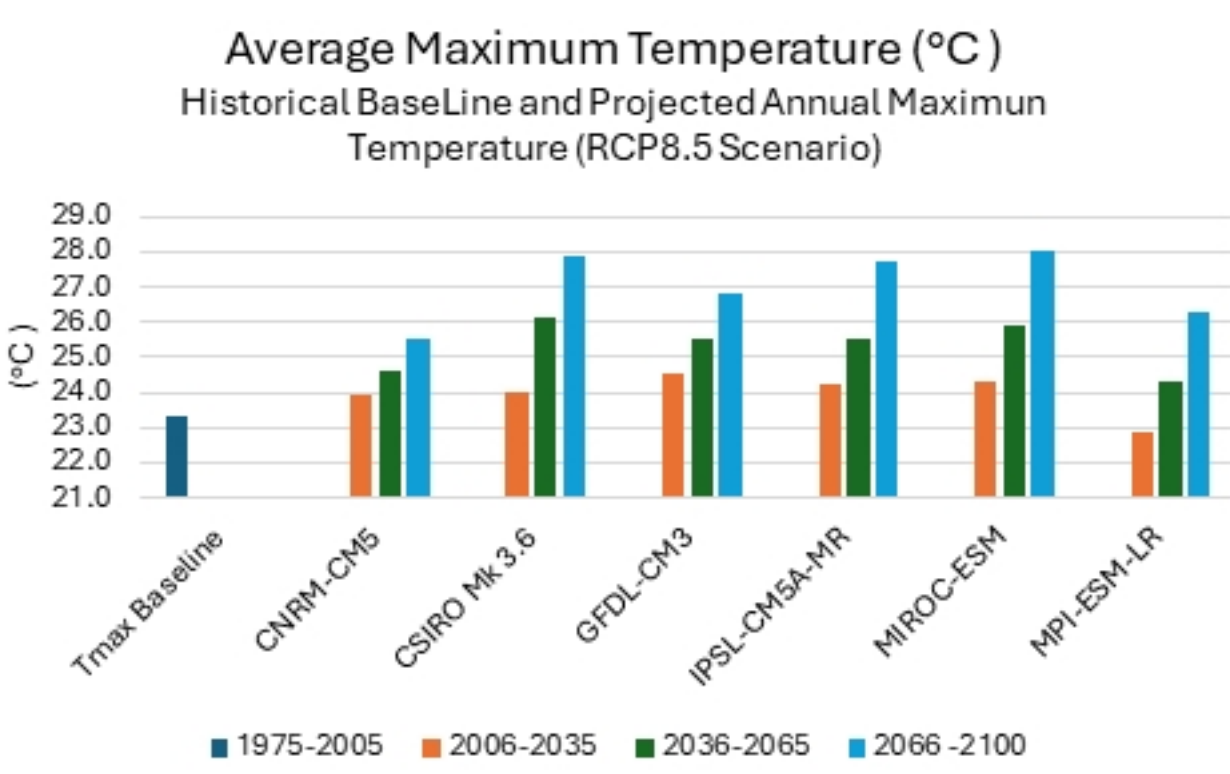
Average Maximum Temperature (°C)
Historical BaseLine and Projected Annual Maximun Temperature (RCP8.5 Scenario)
(°C)
29.0
28.0
27.0
26.0
25.0
24.0
23.0
22.0
21.0
Tmax Baseline
CNRM-CM5
CSIRO Mk 3.6
GFDL-CM3
IPSL-CM5A-MR
MIROC-ESM
MPI-ESM-LR
1975-2005
2006-2035
2036-2065
2066 -2100

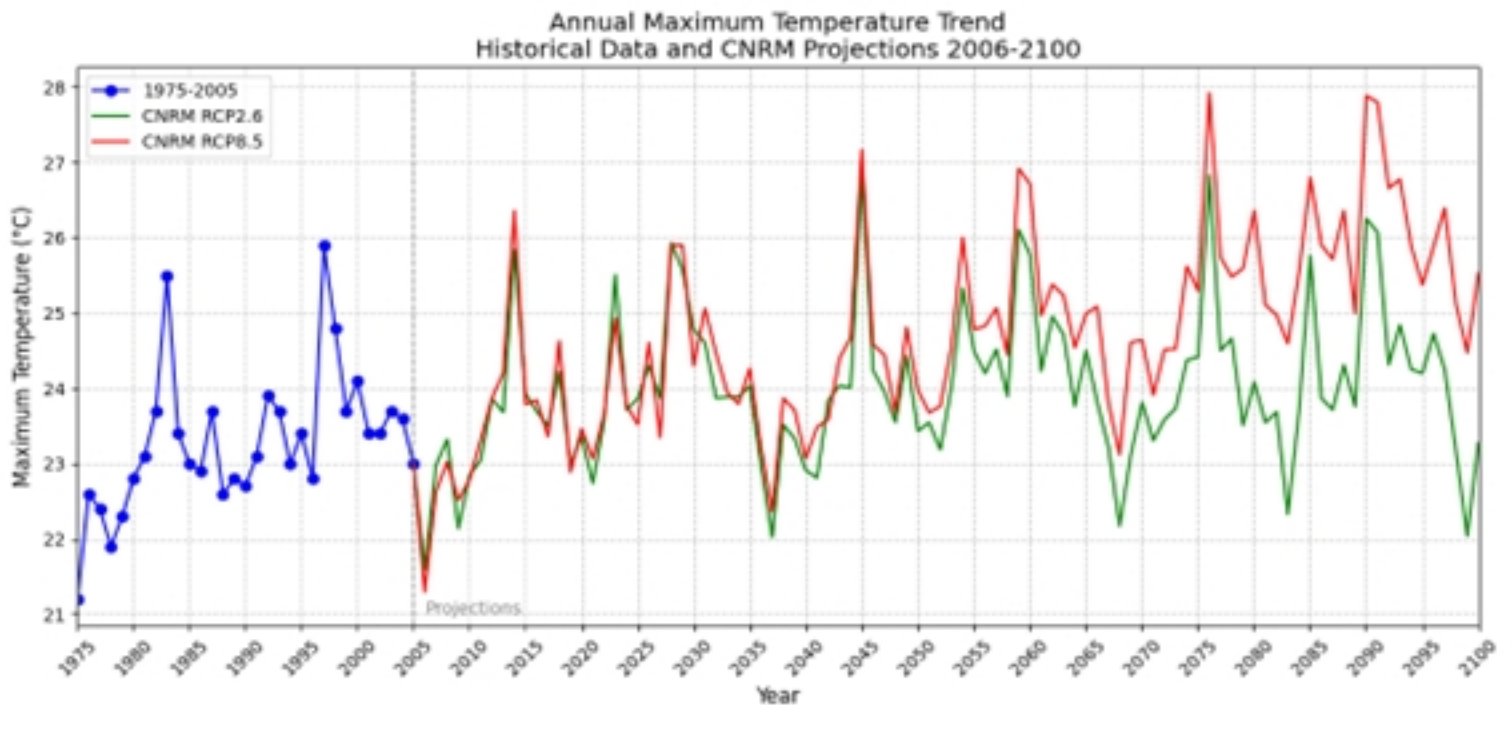
Annual Maximum Temperature Trend
Historical Data and CNRM Projections 2006-2100
1975-2005
CNRM RCP2.6
CNRM RCP8.5
Projections
Maximum Temperature (°C)
Year
21
22
23
24
25
26
27
28
1975
1980
1985
1990
1995
2000
2005
2010
2015
2020
2025
2030
2035
2040
2045
2050
2055
2060
2065
2070
2075
2080
2085
2090
2095
2100

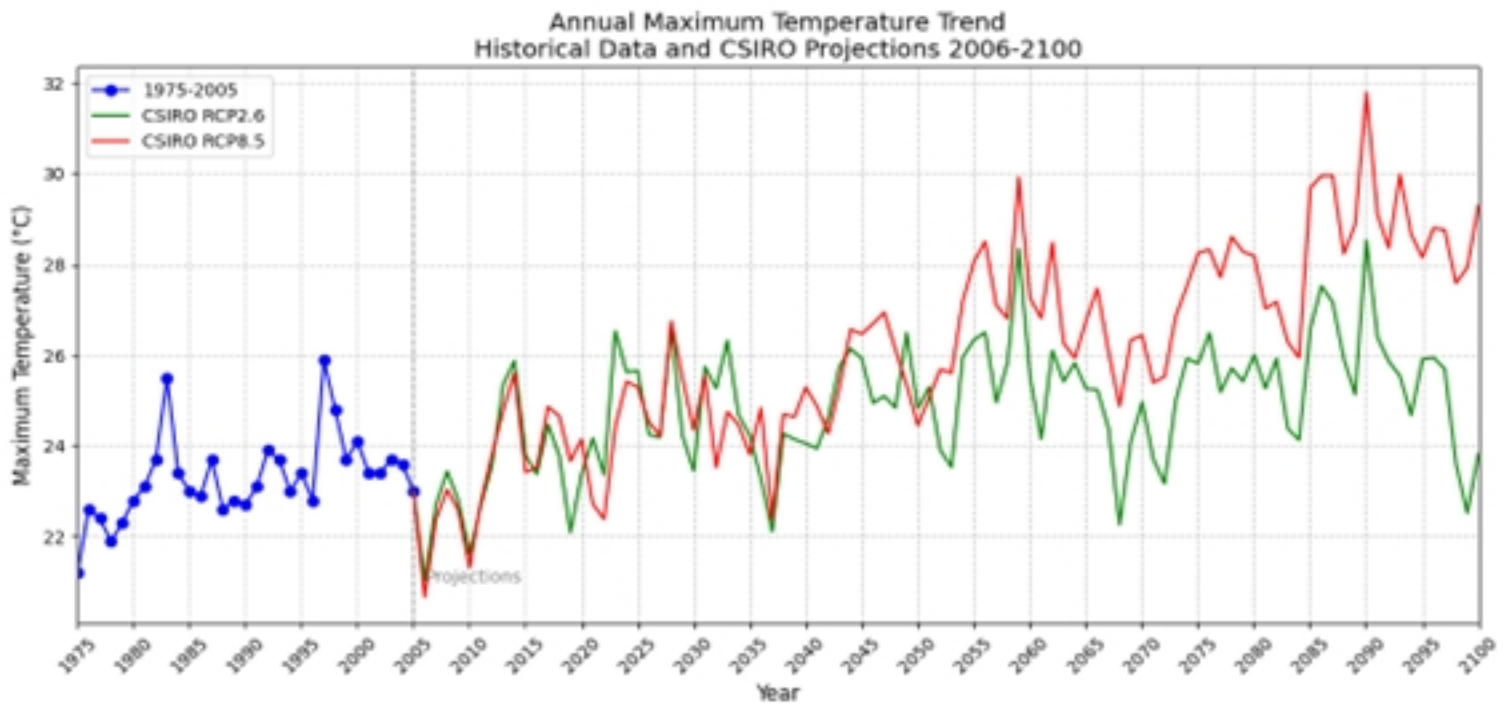
Annual Maximum Temperature Trend
Historical Data and CSIRO Projections 2006-2100
1975-2005
CSIRO RCP2.6
CSIRO RCP8.5
Maximum Temperature (°C)
Year
Projections

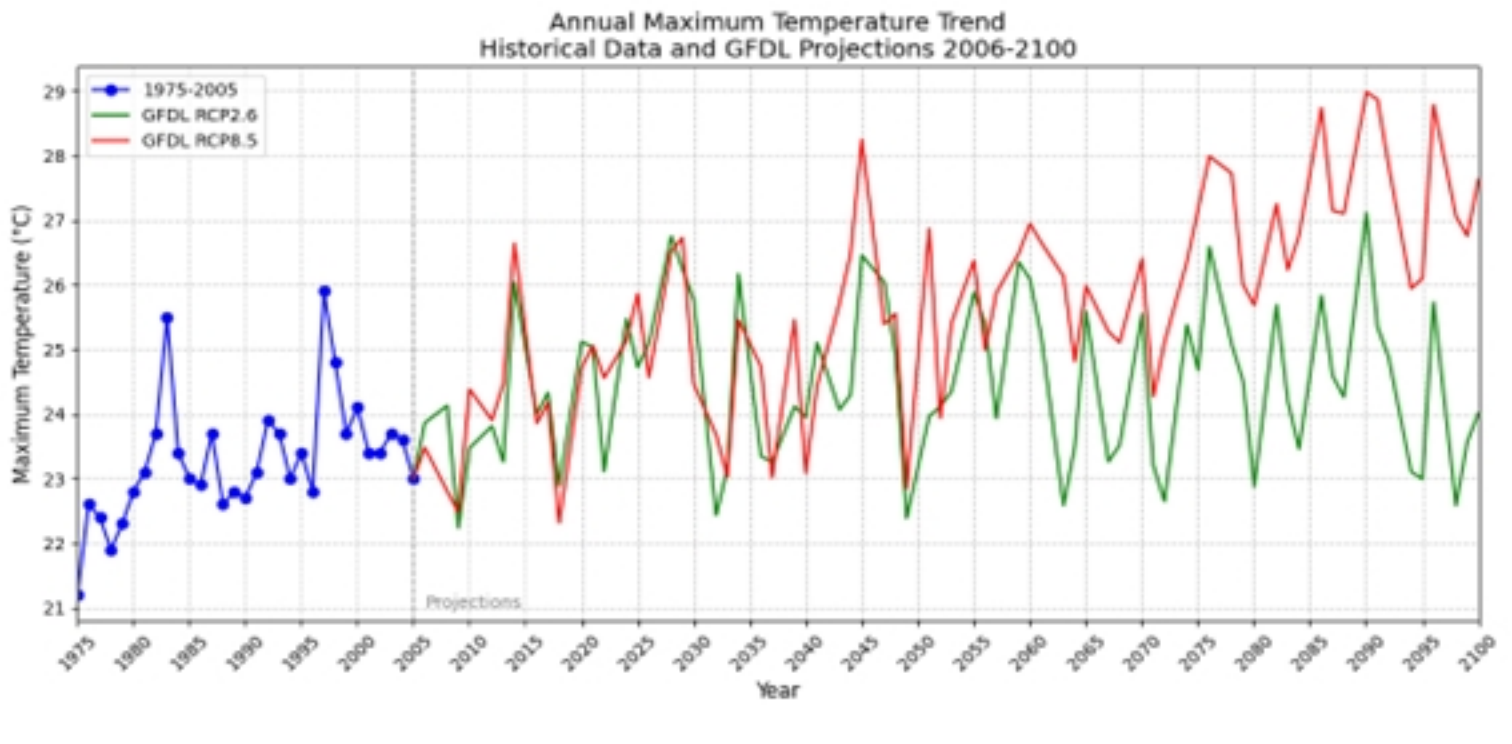
Annual Maximum Temperature Trend
Historical Data and GFDL Projections 2006-2100
1975-2005
GFDL RCP2.6
GFDL RCP8.5
Projections
Maximum Temperature (°C)
Year
21
22
23
24
25
26
27
28
29
1975
1980
1985
1990
1995
2000
2005
2010
2015
2020
2025
2030
2035
2040
2045
2050
2055
2060
2065
2070
2075
2080
2085
2090
2095
2100

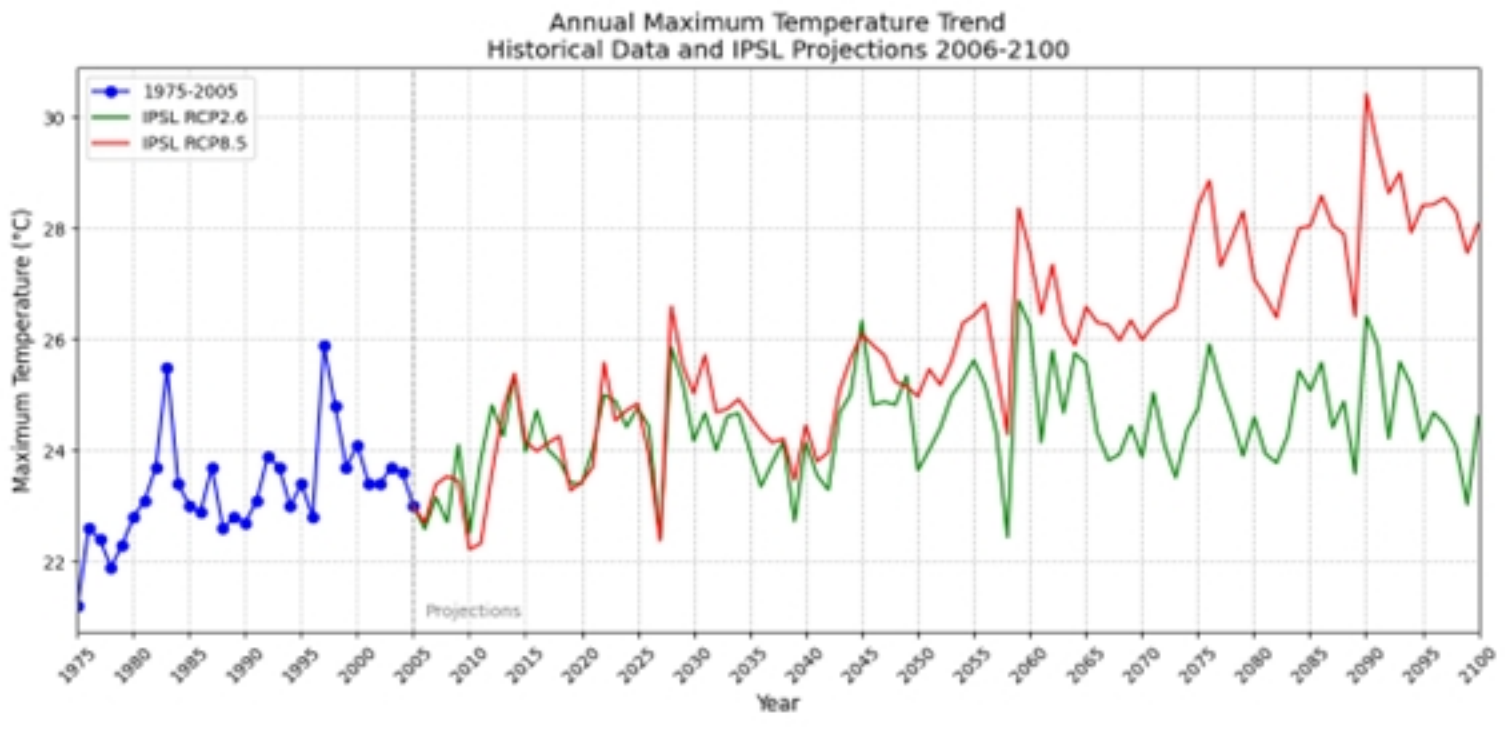
Annual Maximum Temperature Trend
Historical Data and IPSL Projections 2006-2100
1975-2005
IPSL RCP2.6
IPSL RCP8.5
Maximum Temperature (°C)
Year
Projections
22
24
26
28
30
1975
1980
1985
1990
1995
2000
2005
2010
2015
2020
2025
2030
2035
2040
2045
2050
2055
2060
2065
2070
2075
2080
2085
2090
2095
2100

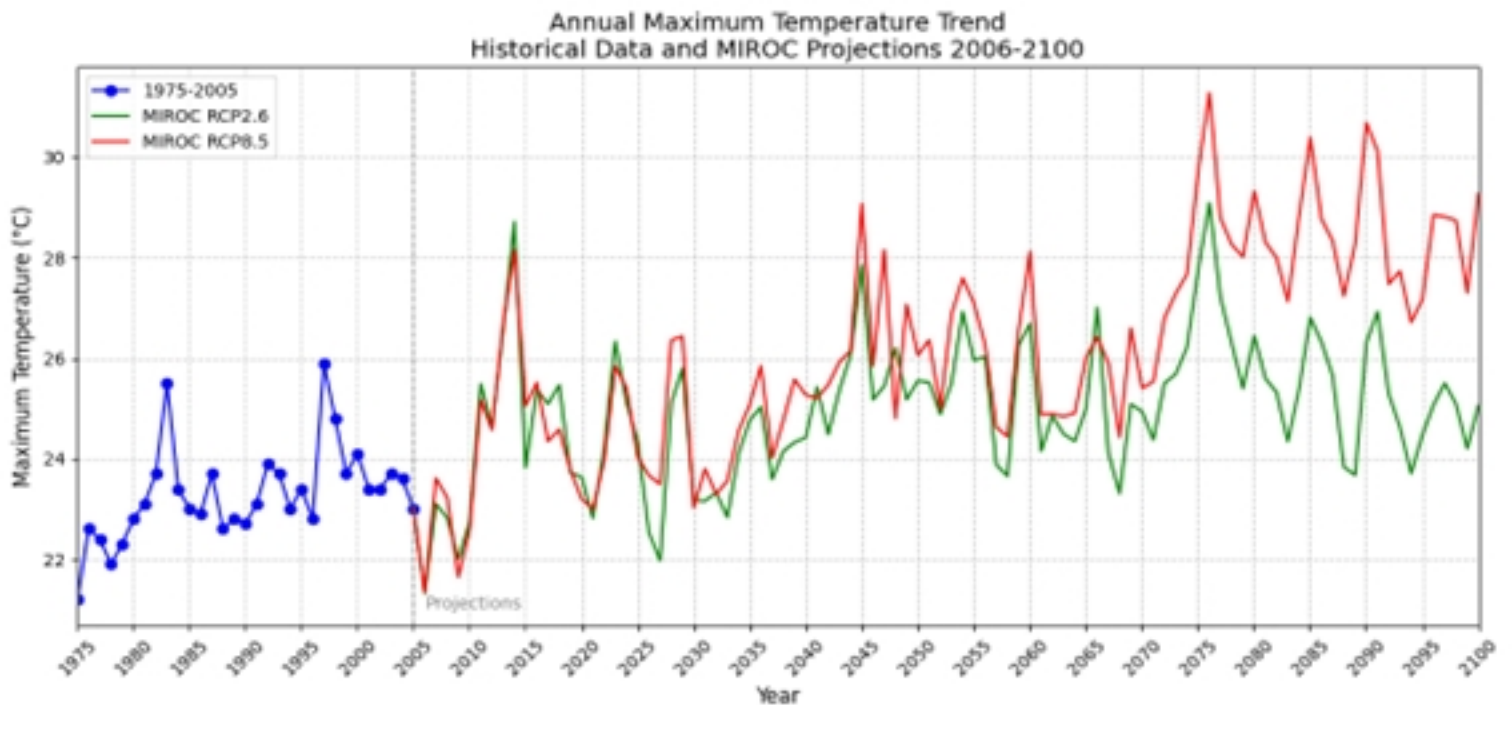
Annual Maximum Temperature Trend
Historical Data and MIROC Projections 2006-2100
1975-2005
MIROC RCP2.6
MIROC RCP8.5
Projections
Maximum Temperature (°C)
Year
22
24
26
28
30
1975
1980
1985
1990
1995
2000
2005
2010
2015
2020
2025
2030
2035
2040
2045
2050
2055
2060
2065
2070
2075
2080
2085
2090
2095
2100

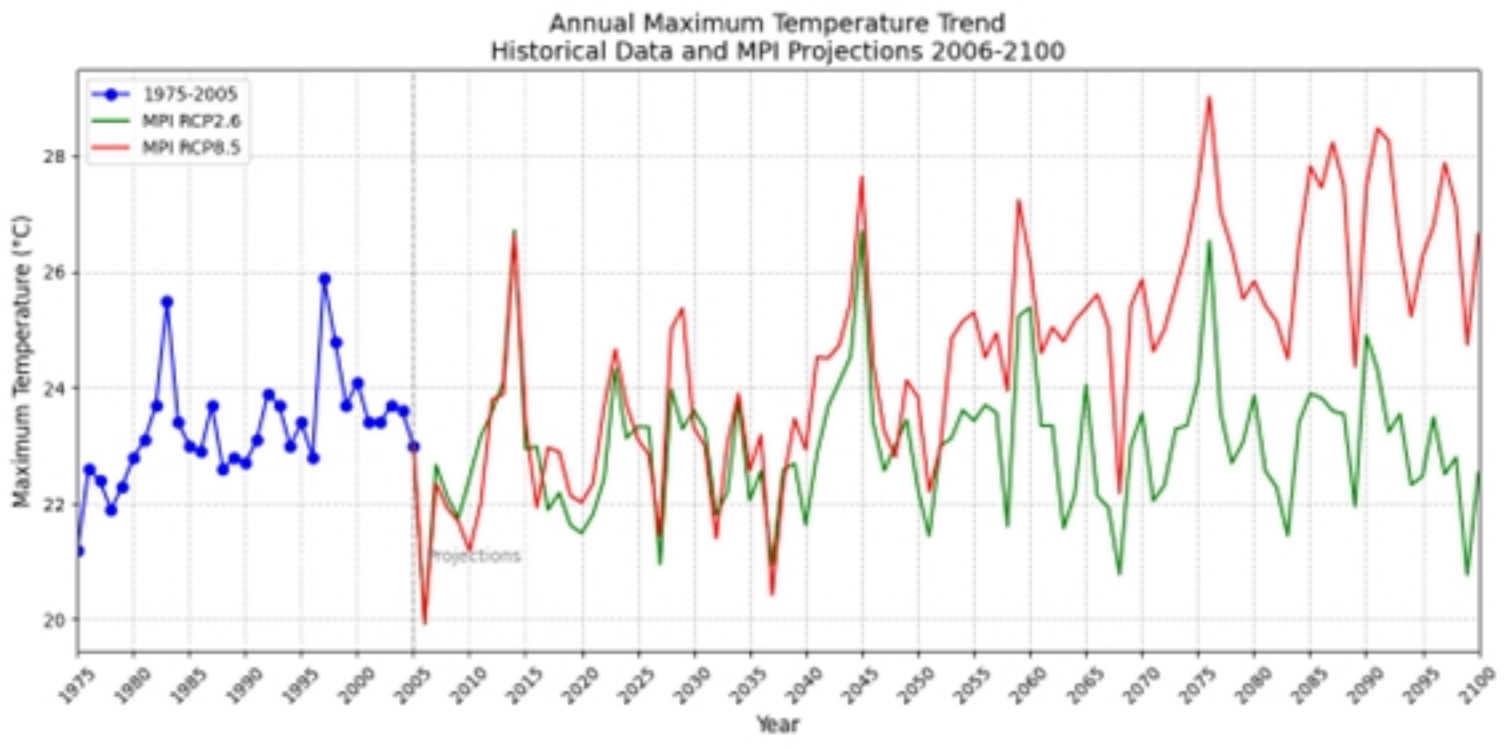
Annual Maximum Temperature Trend
Historical Data and MPI Projections 2006-2100
1975-2005
MPI RCP2.6
MPI RCP8.5
Projections
Maximum Temperature (°C)
Year
20
22
24
26
28
1975
1980
1985
1990
1995
2000
2005
2010
2015
2020
2025
2030
2035
2040
2045
2050
2055
2060
2065
2070
2075
2080
2085
2090
2095
2100